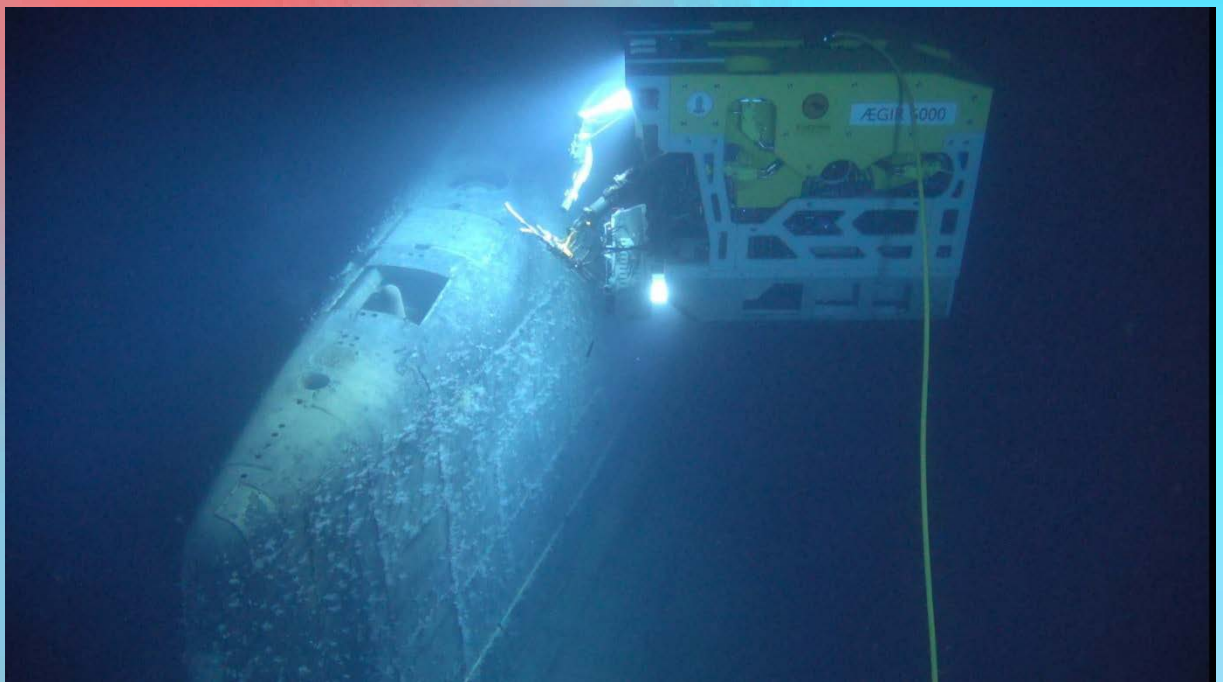


Dispersion of Radioactive Contaminants from the Komsomolets Submarine

Dispersion of Radioactive Contaminants from the Komsomolets Submarine under Climate and Environmental Change Scenarios



Referanse

Dowdall M, Karcher M*, Kauker F*, Standingr WJF. Spredning av radioaktive forurensninger fra Komsomolets-ubåten under scenarier for klima- og miljøendringer. DSA-rapport 2024: nr. Østerås, Direktoratet for strålevern og atomsikkerhet, 2025.

*O.A.Sys - Ocean Atmosphere Systems GmbH Teweesteg 4, D-20249 Hamburg, Germany

Published 2025-12-16
Pages 49
Front photo: Institute of Marine Research
DSA,
Postboks 55,
No-1332 Østerås,
Norge.

Emneord

Komsomolets ubåt, klimaendringer, spredning av forurensninger.

Telephone 67 16 25 00

Resymé

De mulige effektene av scenarier for klimaendringer på potensiell spredning av radioaktive stoffer fra Komsomolets-ubåten ble undersøkt for områder langs den nordlige norskekysten. Alle forsøk resulterte i redusert blanding og konveksjon som førte til et lavere potensial for dypvannsutslipp for å nå overflatevann. Forstyrrelseseksperimentene for klimaendringer indikerer en redusert vertikal blanding og konveksjon i Norskehavet, og reduserer dermed vertikal blanding av sporstoffet, noe som fører til lavere overflatesporkonsentrasjoner og lavere sporstoffinnhold på øvre nivå sammenlignet med de uforstyrrede grunnlinjeforsøkene.

Email dsa@dsa.no
dsa.no

ISSN 2535-7339

Reference

Dowdall M, Karcher M*, Kauker F*, Standingr WJF. Dispersion of Radioactive Contaminants from the Komsomolets Submarine under Climate and Environmental Change Scenarios. DSA-rapport 2024:nr. Østerås, Direktoratet for strålevern og atomsikkerhet, 2025.

*O.A.Sys - Ocean Atmosphere Systems GmbH Teweesteg 4, D-20249 Hamburg, Germany

Language: English.

Key words

Komsomolets submarine, climate change, dispersal of contamination

Abstract

The potential effects of climate change scenarios on potential dispersal of contaminants from the Komsomolets submarine was explored for points along the northern Norwegian coast. All experiments resulted in reduced mixing and convection leading to a lower potential for deep water release to reach surface waters. The climate change perturbation experiments indicate a reduced vertical mixing and convection in the Nordic Seas, thus reducing vertical mixing of the tracer, leading to lower surface tracer concentrations and lower upper-level tracer content in comparison to the unperturbed baseline experiments.

Project Manager: Mark Dowdall.

Godkjent:



Sara Skodbo, Deputy Director General, International Nuclear Safety and Security, and R&D Department

Dispersion of Radioactive Contaminants from the Komsomolets Submarine under Climate and Environmental Change Scenarios.

Innholdsfortegnelse

1	Introduction	5
1.1	Komsomolets submarine	5
1.1.1	Climate change	7
2	Model experiments	11
2.1	Rationale for the scenario constructions	11
2.2	Decadal trends of atmospheric conditions in the Arctic 1982-2021	11
2.3	Climate change scenario: experimental design	15
2.4	Release scenarios	18
2.5	Model description	20
2.6	Scenario experiments	21
2.6.1	Scenario experiments for continuous bottom release	21
2.6.2	Scenario experiments for continuous whole column release	28
2.6.3	Scenario experiments for instantaneous bottom release	34
2.6.4	Scenario experiments for instantaneous whole column release	39
3	Conclusions	45
4	References	46

1 Introduction

The report was funded through the Norwegian Nuclear Action plan with yearly allocations to DSA from the Norwegian ministry of Foreign Affairs. It gives knowledge about potential impact following scenarios affecting radioactive material in the Russian nuclear submarine Komsomolets.

1.1 Komsomolets submarine

The Russian nuclear submarine “Komsomolets” (K-278) sank on the 7th of April 1989 as a consequence of a fire onboard the vessel which now lies at 1673 m to the southwest of Bear Island in the Norwegian Sea (73°43'16" N, 13°16'52" E). The sinking resulted in the loss of 42 of the crew. The submarine was powered by one 190 MW OK-650b-3 PWR which was shut down early during the progression of the accident. The vessel had two nuclear torpedoes onboard at the time of the sinking (Gladkov et al., 1994). The total inventory of the reactor at the time of sinking is estimated to have been 29 PBq with 16 TBq of $^{239,240}\text{Pu}$ contained within the two nuclear warheads (Gladkov et al., 1994; Høibraaten et al., 1997). As of 2019, the residual activity in the reactor (~ 3 PBq) is almost entirely due to the isotopes ^{137}Cs and ^{90}Sr .

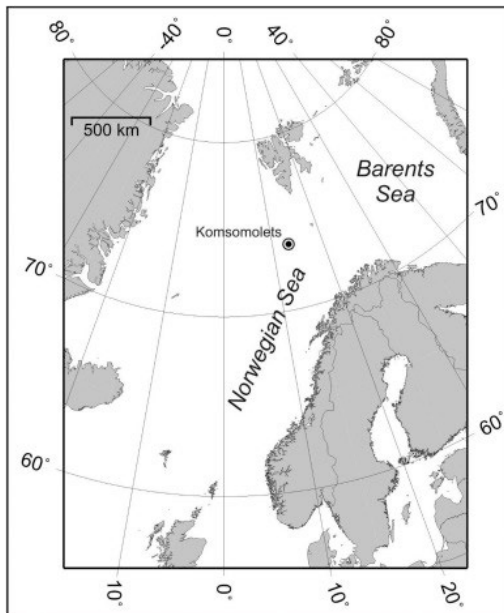


Figure 1: Map depicting the location of the sunken submarine ‘Komsomolets’ at 1673 m depth (Gwynn et al, 2018)

The status of the submarine and contamination of its environs have been investigated during several expeditions conducted between 1989 and 2019. These expeditions have been conducted by Soviet and, subsequently, Russian authorities and institutes with some investigations having been conducted by expeditions from Norway, Germany and the United Kingdom, details of which may be found in Sivintsev et al., (2005). Damage to both outer and inner pressure hulls has been reported over the torpedo compartment, and it has been reported that the nuclear material of the warheads were exposed to seawater (Yablokov et al., 1993). Releases of radionuclides (^{60}Co , ^{134}Cs and ^{137}Cs) from the submarine via a ventilation duct have been reported (see: Nejdánov, 1993; Gladkov et al., 1994 and Kazennov 2010). Reported concentrations of ^{137}Cs in the duct (as of 1994) were of the order of 1 MBq/m^3 with a decrease to 4 kBq/m^3 in the area around the ducts opening (Gladkov et al., 1994). Annual releases of ^{137}Cs from the submarine were estimated to be of the order of 500 GBq/yr (Gladkov et al., 1994). By 2007, releases of ^{137}Cs from the duct were reported to have decreased (Kazennov, 2010), Vysotsky et al. (2014) providing estimates of ^{137}Cs and ^{90}Sr releases of 0.1 GBq/yr . The most recent data for conditions at the wreck site

indicate that activity concentrations of ^{137}Cs in seawater drawn from inside the duct range from <8.0 to 857 Bq/l which provides indications that the reactor is still releasing radionuclides and that these releases exhibit variability with respect to the amount being released and the duration of those releases. appear to vary in activity and duration (Heldal et al., 2019). Previous studies (Høibraaten et al., 1997) have indicated a limited potential for significant long-range marine dispersal of contaminants from the Komsomolets submarine while admitting to several uncertainties in their approach.

While the actual or potential impacts for the environment because of leakage and transport of radioactive contaminants from the Komsomolets submarine are in all probability very low at points distant from the wreck site, the ability to make predictions or estimates of dispersal is reliant on an understanding of the relevant environmental conditions. It is well established that the world's oceans are vulnerable to climate change predictions in a number of ways and the potential exists for climate change impacts to have some influence on the dispersion of contamination from the submarine. In this context, the dispersal of contaminants from the submarine was investigated from a climate change standpoint with a view towards elucidating what implications such changes may have on dispersion of contamination from the submarine.

1.1.1 Climate change

While long-term increases in surface temperatures are a development that has been solidly projected by a number of climate models which contributed to the latest IPCC assessment report (IPCC, 2021), the internal variability of the Earth's climate system inevitably leads to a great deal of uncertainty in terms of developments when focusing on the next two decades, especially at the higher latitudes. The context of the present study is therefore to identify those changes in observed atmospheric conditions in recent decades that are attributable to climate change and particularly those that could affect vertical mixing properties. These changes are then assumed to continue to occur over the next two decades and form the basis for a series of sensitivity experiments to identify possible changes in the dispersion of a hypothetical release of contaminants from the submarine. As a start point, atmospheric changes that have occurred over the last 40 years are identified through statistical analysis of atmospheric reanalysis data from two reanalysis datasets: CFS-R/v2 (Saha et al., 2010, 2011) and ERA5 (Hersbach et al., 2020). The changes observed between the 1982-2001 and 2002-2021 periods, multiplied by a factor of 1 and 2, respectively, are then superimposed on the unperturbed forcing of the two periods to mimic the increasing atmospheric changes assumed to occur for these variables over the next two decades. The factors of 1 and 2 thereby stand for two intensities of change. This exercise was intentionally performed with each of the two time periods as a baseline to examine the impact of possible future climate change perturbations acting on conditions when the effects of climate change were not as pronounced as in recent years.

Figures 2, 3 and 4 show examples of projected changes in the atmosphere (globally and in the Arctic) as they are resulting from the CMIP6 model experiments for the IPCC's sixth assessment (IPCC, 2021). The black curves show the historical development until 2015, and the coloured curves show the projected development for different climate change scenarios. While there are clearly distinguishable long-term trends for the different scenarios on century long time scales, the scenarios for the next two decades are not very clearly separated. Therefore, extrapolating the trends of the last decades is a reasonable estimate for the variables presented.

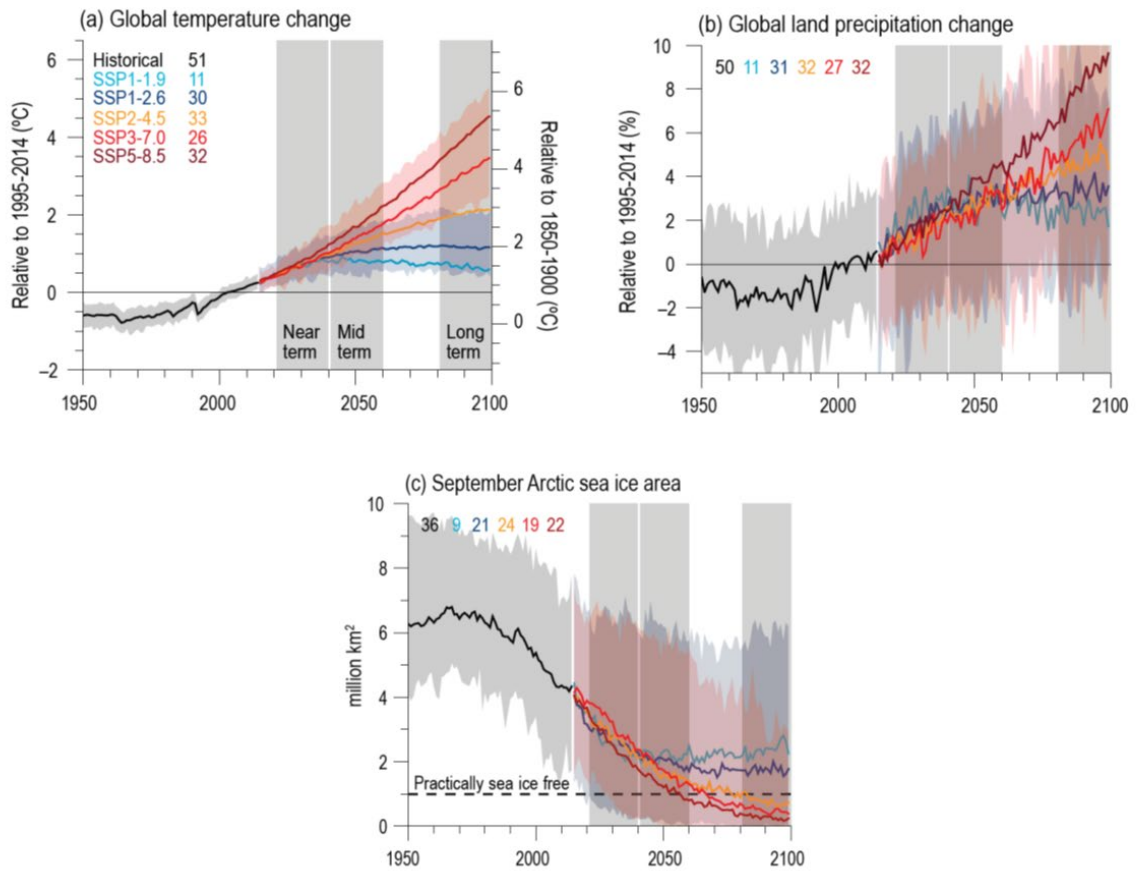


Figure 2. (from IPCC, 2021) Graphical depiction of selected indicators of global climate change from CMIP6 historical and scenario simulations. (a) Global surface air temperature changes relative to the 1995–2014 average (left axis) and relative to the 1850–1900 average. (b) Global land precipitation changes relative to the 1995–2014 average. (c) September mean Arctic sea ice area. In (a–c), the curves show averages over the CMIP6 simulations, the shadings around the SSP1 2.6 and SSP3 7.0 curves show 5–95% ranges, and the numbers near the top show the number of model simulations used. Results are derived from concentration-driven simulations. (Further details on data sources and processing are available in the chapter data table, in IPCC (2021) Table 4SM.1).

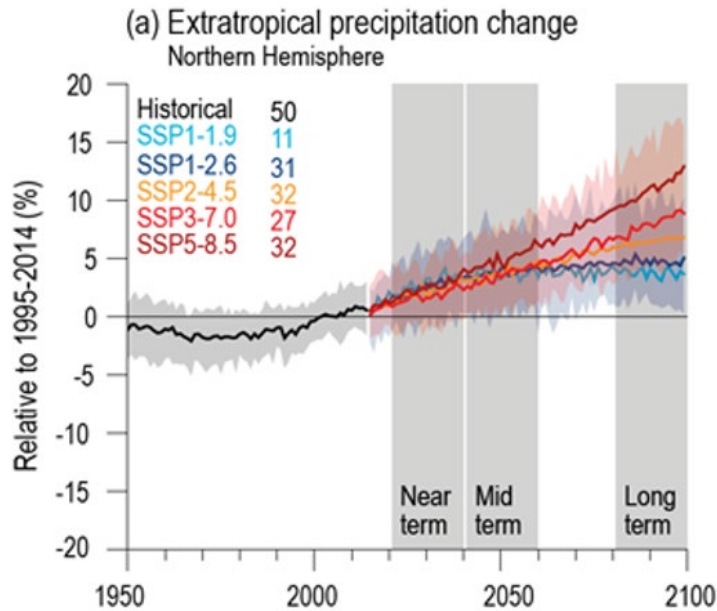


Figure 3 (from IPCC, 2021) Graphical depiction of CMIP6 annual mean precipitation changes (%) from historical and scenario simulations. (a) Northern Hemisphere extra-tropics (30°N–90°N). Changes are relative to 1995–2014 averages. Displayed are multi-model averages and, in parentheses, 5–95% ranges. The numbers inside each panel are the number of model simulations. Results are derived from concentration-driven simulations. (Further details on data sources and processing are available in the chapter data table, in IPCC (2021) Table 4.SM.1).

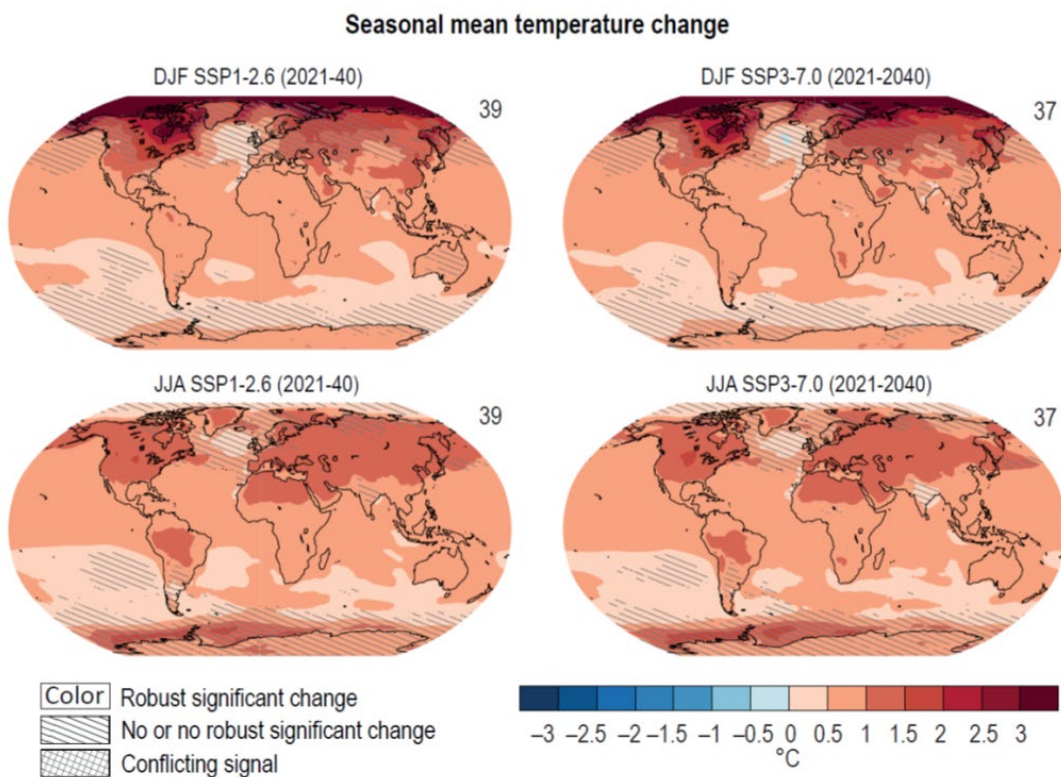


Figure 4: (from IPCC, 2021) Maps of near-term change of seasonal mean surface temperature. Displayed are projected spatial patterns of CMIP6 multi-model mean change (°C) in (top) December–January–February (DJF) and (bottom) June–July–August (JJA) near-surface air temperature for 2021–2040 from

SSP1 2.6 and SSP3 7.0 relative to 1995–2014. The number of models used is indicated in the top right of the maps. No overlay indicates regions where the change is robust and likely emerges from internal variability, that is, where at least 66% of the models show a change greater than the internal-variability threshold (IPCC, 2021, Section 4.2.6) and at least 80% of the models agree on the sign of change. Diagonal lines indicate regions with no change or no robust significant change, where fewer than 66% of the models show change greater than the internal-variability threshold. Crossed lines indicate areas of conflicting signals where at least 66% of the models show change greater than the internal-variability threshold but fewer than 80% of all models agree on the sign of change. Further details on data sources and processing are available in the chapter data table (IPCC, 2021, Table 4.SM.1).

Targeted studies on the effects of climate change on vertical ocean mixing in the Arctic are sparse. To investigate the hypothesised increase in mixing in high northern latitudes, particularly under previously ice-covered parts of the ocean, Liang and Losch (2018) performed a series of sensitivity experiments with prescribed increased mixing. The rationale was that due to reduced sea ice cover, there would be increased mixing as a result of increased new ice formation in winter (promoting the release of brine) and increased wind stirring in the upper ocean in now ice-free areas. As expected, they found that an increased vertical mixing (artificially imposed) will enhance vertical heat and salinity exchange.

Consequently, the decreased vertical temperature and salinity gradients of the upper Arctic Ocean leads to a weaker stratification, which makes the heat of the Atlantic Water layer accessible to the surface layer, contributing to an increased melting of the sea ice. On the other hand, they identify stronger Arctic Ocean stratification due to increased freshwater input in the Eurasian Basin e.g. during melting of sea ice. In the Nordic Seas, at the location of the sunken submarine, convection is a key factor for the vertical mixing of water masses and thus impacting the vertical dispersion of potentially release radionuclides strongly. Climate change impacting convection events, e.g. due to increased stratification in regions not covered by sea ice (anymore), could modify the frequency, location, and depth of convection events. The recent observed sea ice retreat in the northern ocean is shown to impact convection already nowadays (Moore et al. 2015; Våge et al. 2018; Latarius and Quadfasel 2016; Lique et al. 2015, 2018).

Wu et al. (2021) use a coupled climate model to investigate the changes in ocean convection in the Nordic Seas which are initiated by climate change. They identify differing response in regions which had previously been covered by sea ice and originally open ocean regions. Regions of sea ice retreat exhibit an increase of vertical mixing in the upper ocean. The cause is a higher heat loss to the atmosphere in the now exposed areas and an enhanced impact of the wind stress now that the ice does not shield the ocean anymore. They claim that this is particularly vivid in case of sudden cold weather event (Papritz and Spengler, 2017). Furthermore, they identify intensified brine rejection to the ocean in regions which can now form new sea ice in winter as a source of reducing stability of the water column. The most pronounced effect they find, though, is away from the region of sea ice retreat, toward the Greenland Sea Gyre where obviously sea ice production is not an important driver for convection (Brakstad et al. 2019). Here the convective depth is slightly reduced as sea ice retreats, but climate warming significantly amplifies this. This remarkable shoaling is due to increased ocean stratification from considerable warming of the upper ocean in agreement with observations (Latarius and Quadfasel 2010; Lauvset et al. 2018; Selyuzhenok et al. 2020).

As sea ice continues to retreat under global warming, we may expect to see a reduction of water mass modification in the central Greenland Sea, because of reduced atmospheric forcing of dense water production (Moore et al. 2015) and considerable upper-ocean warming. This would decrease the production of Greenland Sea Intermediate Water, which had become the main product of convection in the Greenland Sea in the recent past (Karstensen et al. 2005; Jeansson et al. 2017).

Mulwijk et al. (2022) investigate the changes in stratification in selected regions of the northern hemisphere projected by the IPCC set of CMIP6 models. They state that observations and simulations

agree that the Arctic Ocean is becoming warmer and that there is ongoing freshening in the Amerasian Basins. The simulations also agree that the observed weakening of the stratification in the Eurasian Basin does not spread eastward into the Amerasian Basin. There is a strong warming of the Atlantic Water layer in the projections. This is consistent with the so-called ‘Atlantification’ (Polyakov et al., 2020). The authors suggest using ΔPE as new indicator of stratification strength. It is defined as an integral measure of the potential energy needed to fully mix the water column from the surface down to a previously determined depth. They state that ‘Temporal change and regional contrasts observed by more traditional stratification definitions (e.g. Polyakov et al. 2020) are captured well by this new parameter, whose definition is not sensitive to model biases.’

Their analysis of the CMIP6 ensemble of models reveals that there is no unanimous trend of stratification that can be derived from the models in the selected four Arctic regions they investigated (Figure 5). An exception is the Beaufort Sea which is projected to increase its stratification in the coming decades.

In the present report ΔPE is used as an indicator for the intensity of stratification in the for this study performed model sensitivity experiments with NAOSIM. It thus serves as a measure of the strength of the impacts of the climate change response experiments on the potential for enhanced or reduced stratification and thus convection induced vertical mixing.

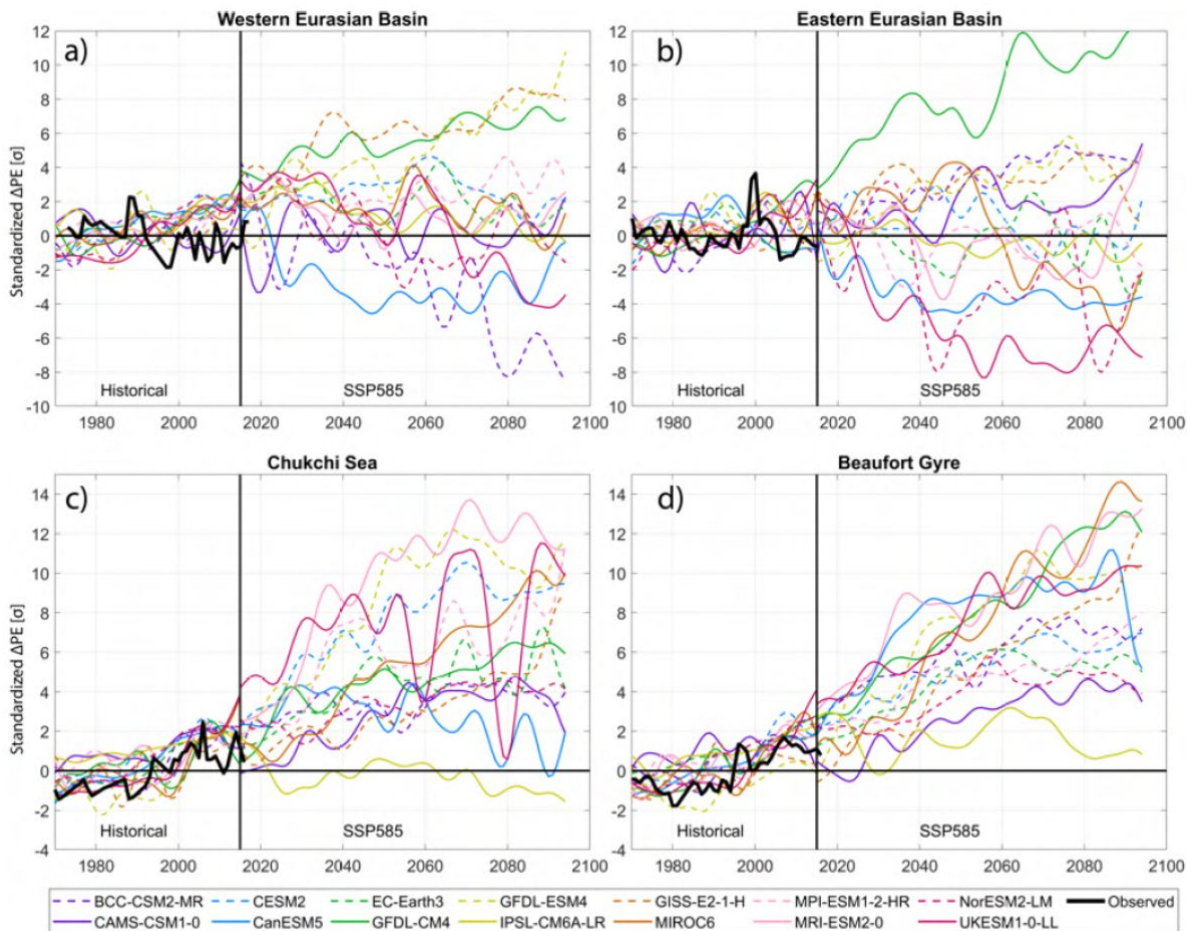


Figure 5: Time series of four regions in the Arctic Ocean (standardized anomalies relative to 1970–2014 mean) of stratification strength, ΔPE [MJ/m²], for 14 CMIP6 models investigated in Mulwijk et al. (2022). More positive values indicate a stronger stratification, i.e. more energy would be needed to mix the water column. All-time series are low-pass filtered with a five year cut-off frequency. Note the different y-axes for the two basins. For comparison, the observed stratification over the period 1970-2017 is plotted in with thick black lines. (Figure from Mulwijk et al. 2022).

2 Model experiments

2.1 Rationale for the scenario constructions

The rationale and design of the model experiments performed for this study is as follows:

- There is a large uncertainty in the predicted atmospheric conditions for the next 2 decades (due to model biases and superposition of long-term trend and internal variability) (IPCC, 2021)
- The report refrains from using IPCC ensemble members to force the experiments, instead trends are identified in the following variables for the past 4 decades from two atmospheric reanalysis datasets: 2m temperature, specific humidity/dew-point temperature, 2m relative humidity, downward longwave radiation, downward shortwave radiation, precipitation, 10-m windspeed.
- Those variables are selected which show a significant trend over this timespan. These are 2m temperature, downward longwave radiation and precipitation.
- Trends are constructed for these variables as the means over time periods of two decades for each of the two atmospheric reanalysis datasets employed.
- The forcing for the model experiments ('our' climate change scenarios) is constructed by superposition of the original atmospheric reanalysis data for each of the two periods with the observed trends, extrapolated into the 'future' with 1x or 2x the amplitude of the observed trend.

2.2 Decadal trends of atmospheric conditions in the Arctic 1982-2021

In the following the results of the statistical analysis of the reanalysis datasets are presented. Only results for those variables which show a statistically significant trend in the two investigated periods (1982-2001 and 2002-2021) are shown. These are:

- 2m temp
- downward longwave radiation
- precipitation

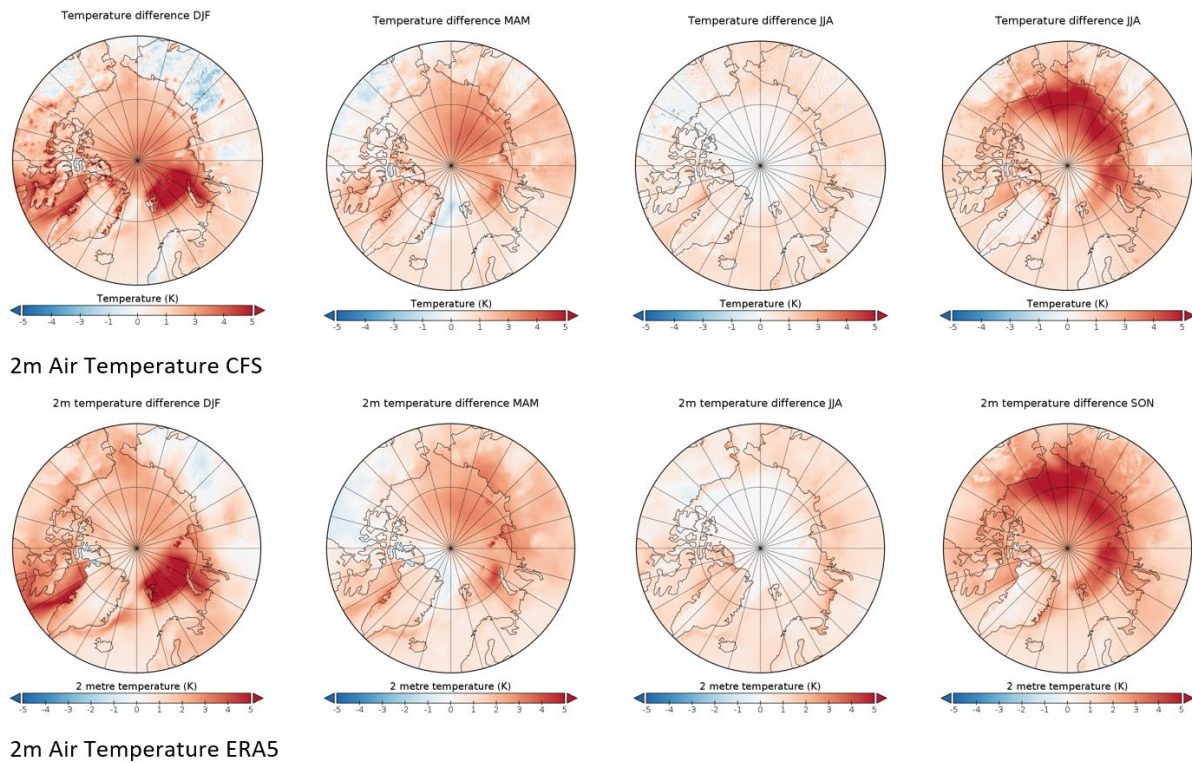


Figure 6: Maps depicting seasonal means of 2 m temperature differences between period 2 (2002-2021) and period 1 (1982-2021) for CFS (top row) and ERA5 (bottom row).

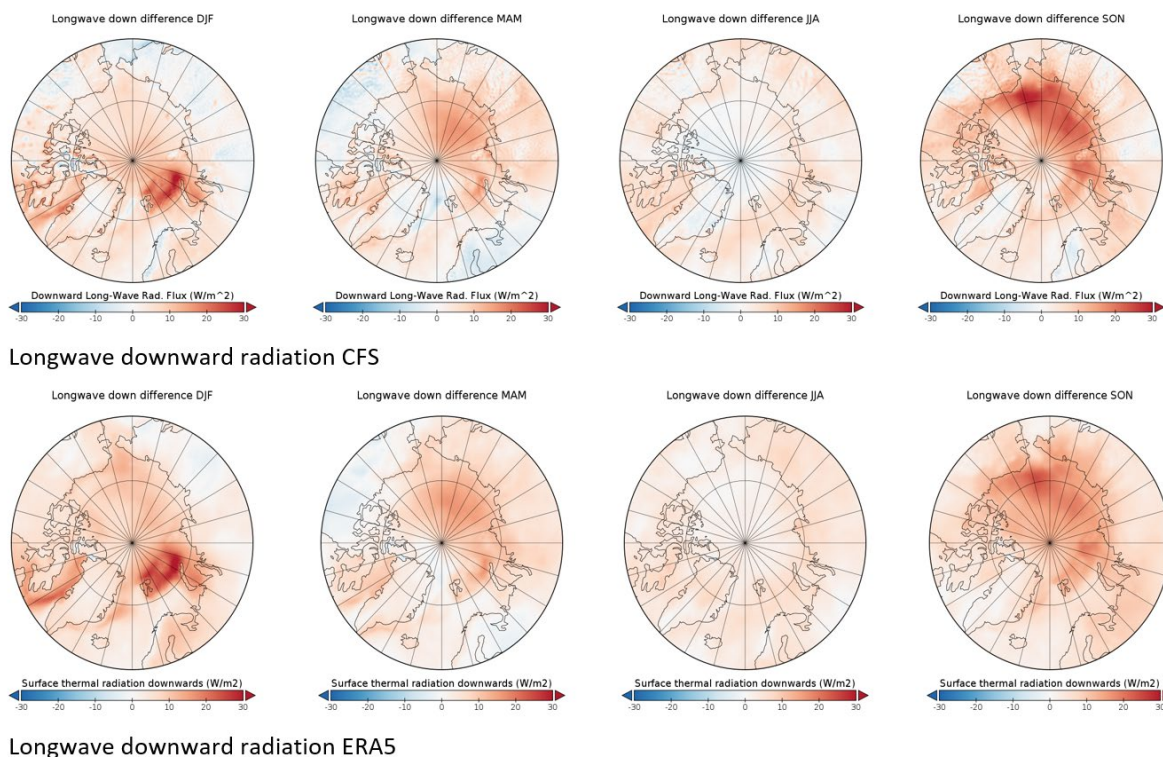


Figure 7: Maps depicting seasonal means of longwave downwelling radiation differences between period 2 (2002-2021) and period 1 (1982-2021) for CFS (top row) and ERA5 (bottom row).

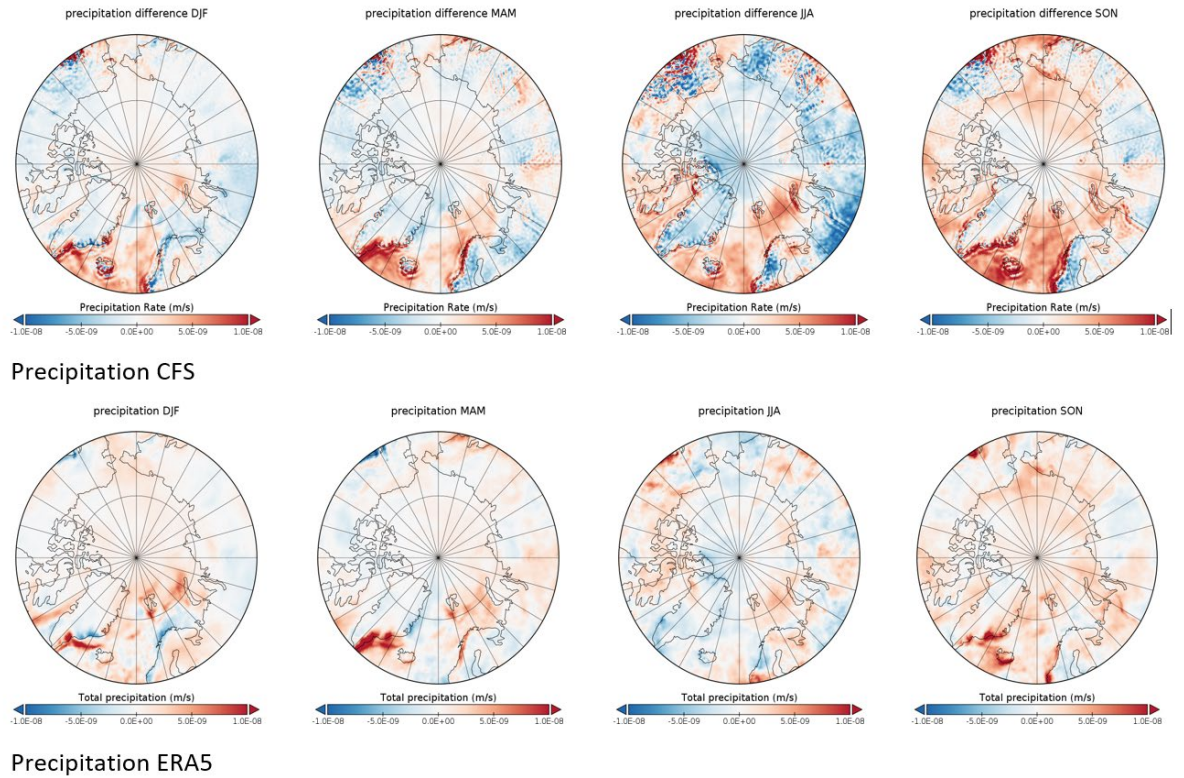


Figure 8: Maps depicting seasonal means of precipitation differences between period 2 (2002-2021) and period 1 (1982-2021) for CFS (top row) and ERA5 (bottom row).

For 2-m temperature (Figure 6) both reanalysis datasets (CFS and ERA5) show a strong warming trend of up to 5 °C in September, October, November (SON) and in December, January, February (DJF) seasons in the Barents Sea, the Siberian Arctic Ocean and the Canadian Arctic Basin. This is mirrored by the downward longwave radiation (Figure 7) showing positive trends up to 20 W/m² in those regions. For precipitation (Figure 8) the two reanalysis datasets agree on an increase in SON in most of the central Arctic basin and the Nordic Seas

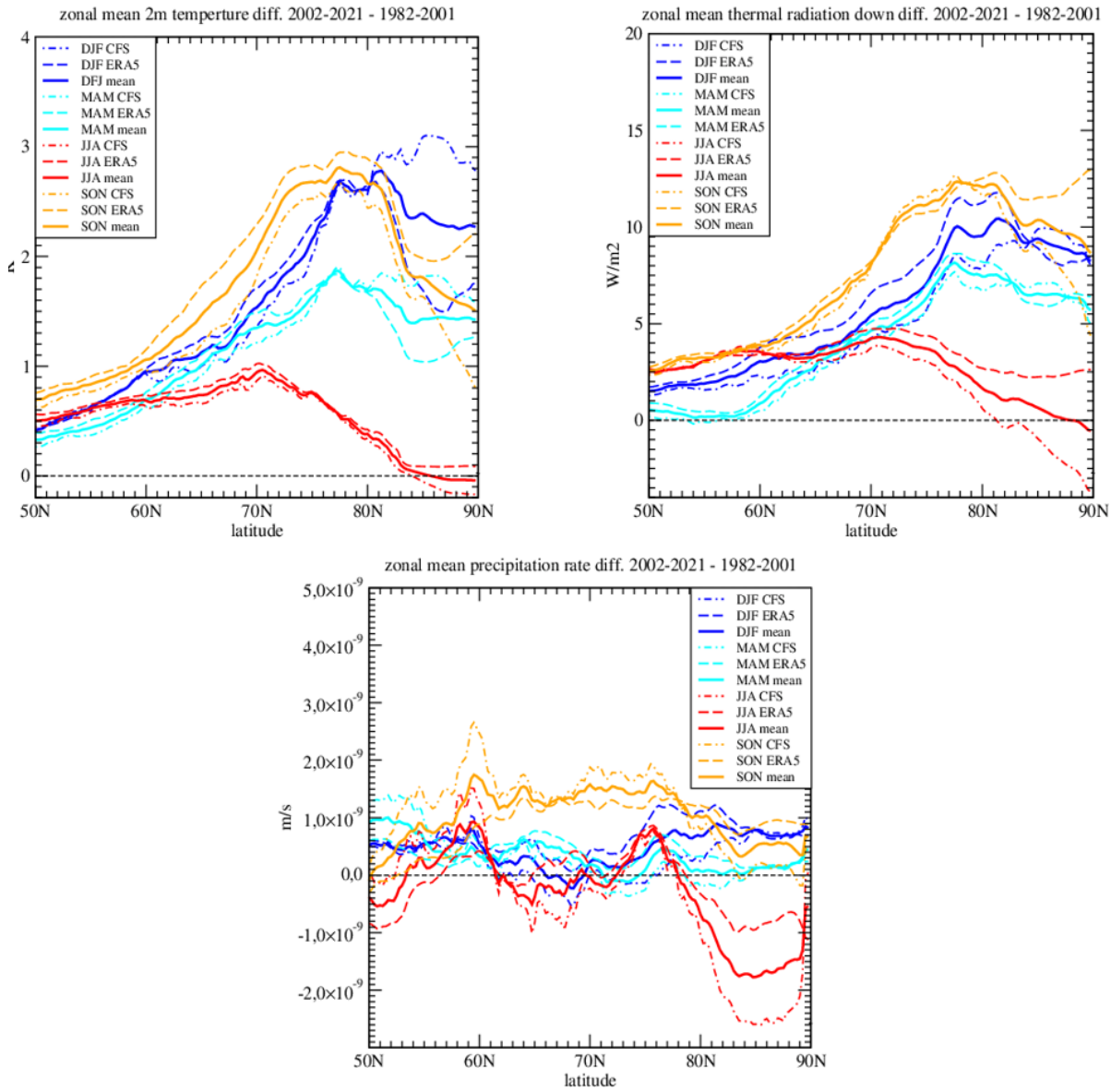


Figure 9: Graphs depicting zonal means of differences between period 2 (2002-2021) and period 1 (1982-2001) and period 2 (2002-2021) for 2m temperature, longwave radiation downward (denoted thermal radiation in the plots), and precipitation rate for forcing dataset CFS (dash-dots), ERA (dash) and mean of the two (solid).

The zonal mean differences for the three variables for each of the four seasons and the two reanalysis datasets between the two periods (Figure 9) show a large similarity of the latitudinal dependency in most cases. The solid thick lines show the mean of the two reanalysis datasets which have been used to force the model experiments.

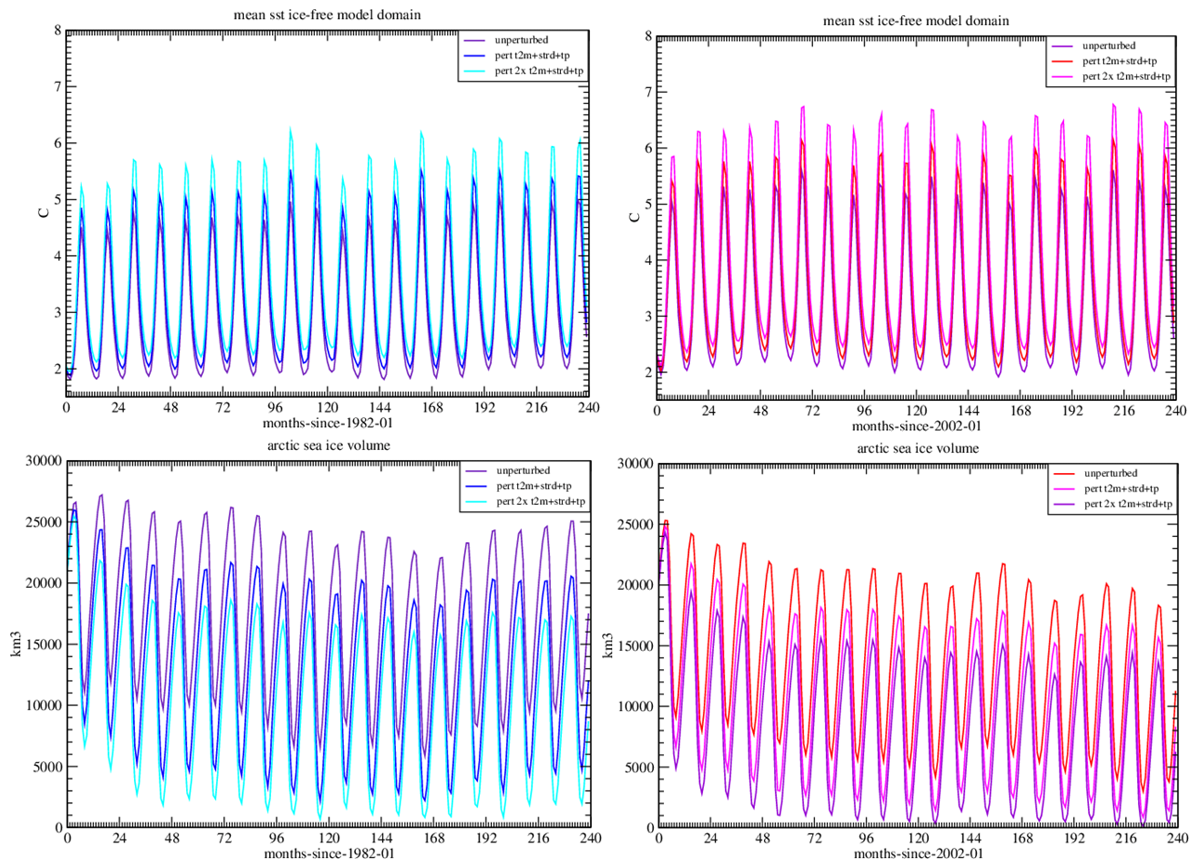


Figure 10: Graphs of surface response to the climate change experiments: SST in the ice-free model domain (top) and Arctic Sea ice volume (bottom). Left: period 1 (1982-2001), right period 2 (2002-2021). Each panel shows monthly means for an unperturbed experiment, an experiment with 1x climate change perturbation and 2x climate change perturbation, respectively.

The surface response in terms of SST in the ice-free domain and the Arctic Sea ice volume (Figure 10) for two decades of unperturbed forcing and climate with 2m-temperature (2mt), surface thermal radiation downwards (strd) and total precipitation (tp) 1 x climate change perturbation and 2 x climate change perturbation superposed, shows an overall increased SST and reduced sea ice volume for both of the periods.

2.3 Climate change scenario: experimental design

Experiments with perturbations of the atmospheric forcing motivated by climate change signals were performed.

The patterns of change for the variables which had exhibited significant trends between period 1 (1982-2001) and period 2 (2002-2021) - 2m temperature, downward longwave radiation and precipitation - were superposed on the respective unperturbed variables in each of the two time periods. The goal is to investigate the response to a climate change signal in the atmospheric forcing that continues the observed trends. Tests were made for the response to perturbations on each single variable as well as on combinations of all three variables. For the main part of the climate change experiments a modified forcing was applied that consisted of a single (1x) perturbation and a doubled (2x) perturbation jointly for all three

atmospheric variables, i.e.: 1 x perturbation of 2m temperature, downward longwave radiation, and precipitation; 2 x perturbation of 2m temperature, downward longwave radiation, and precipitation

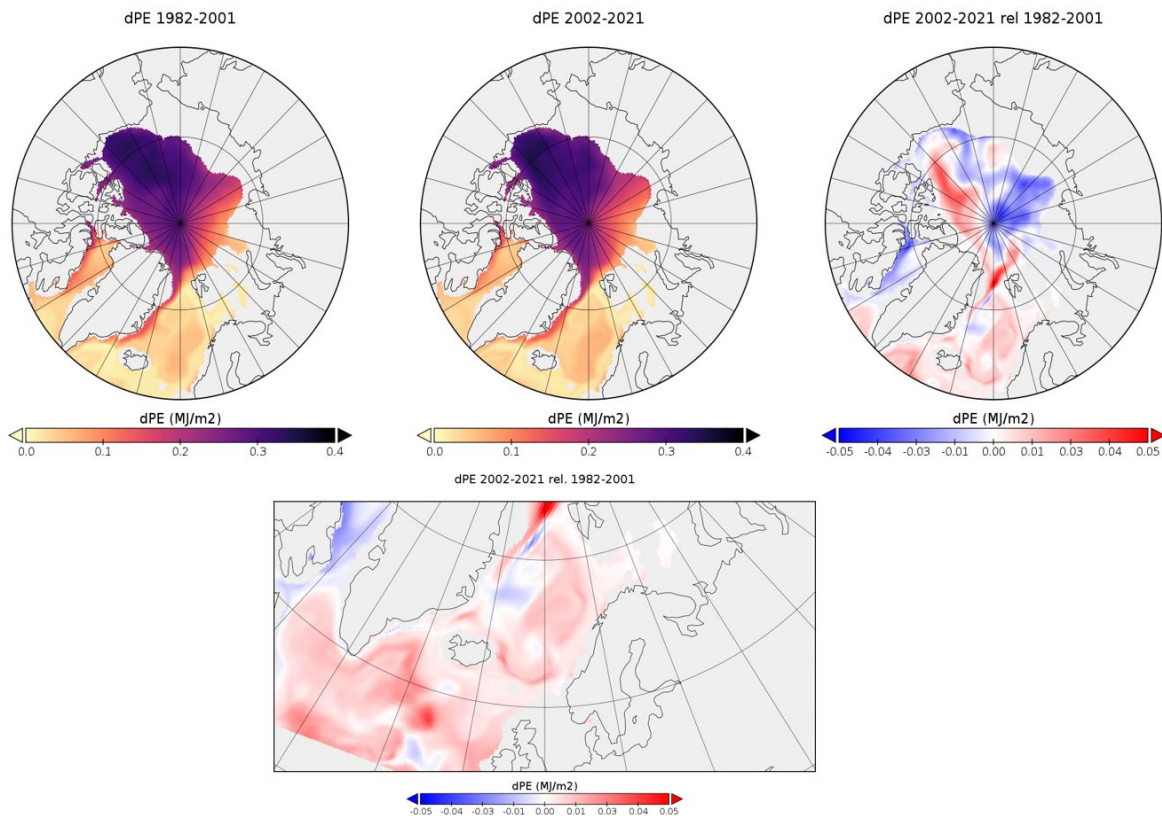
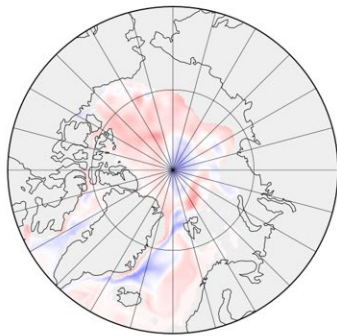


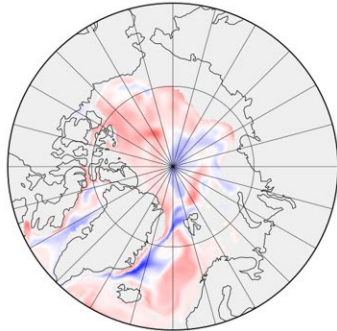
Figure 11: Maps of stratification strength (ΔPE , MJ/m²) for baseline experiments (unperturbed forcing) for period 1 (1982-2001) (left), period 2 (2002-2021) (middle), and difference between period 2 and period 1 (right, bottom with zoom into Nordic Seas), see section 3 for explanation of ΔPE .

For the unperturbed baseline experiments (Figure 11) we find an intensified stratification (increased ΔPE) comparing period 2 with period 1 in the Northern North Atlantic, most of the Nordic Seas and parts of the Canadian Arctic Basin. We identify intensified stratification in the region of the submarine location at the slope of the Barents Sea in the Norwegian Sea.

dPE 1982-2001 - pert t2m+strd+tp fac1 anom

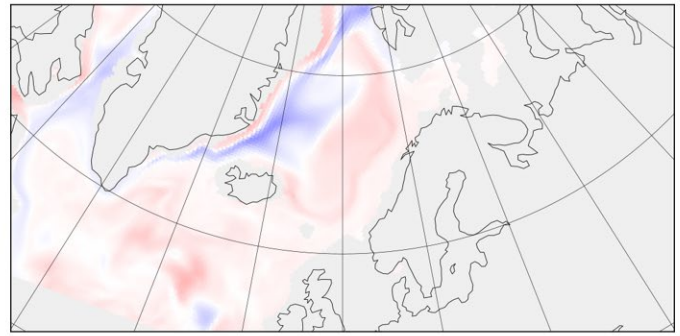


dPE (MJ/m²)
-0.05 -0.04 -0.03 -0.01 0.01 0.03 0.04 0.05
dPE 1982-2001 - pert t2m+strd+tp fac2 anom

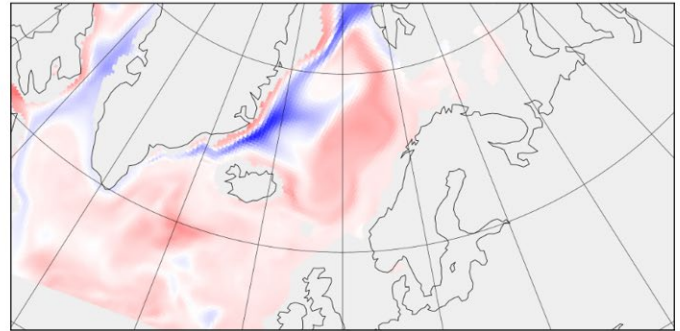


dPE (MJ/m²)
-0.05 -0.04 -0.03 -0.01 0.01 0.03 0.04 0.05

dPE 1982-2001 - pert t2m+strd+tp fac1 anom



dPE (MJ/m²)
-0.05 -0.04 -0.03 -0.01 0.01 0.03 0.04 0.05
dPE 1982-2001 - pert t2m+strd+tp fac2 anom

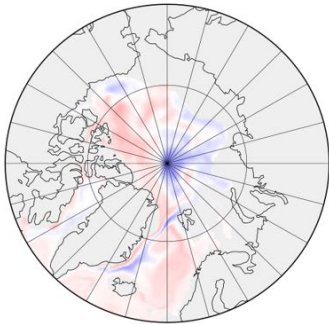


dPE (MJ/m²)
-0.05 -0.04 -0.03 -0.01 0.01 0.03 0.04 0.05

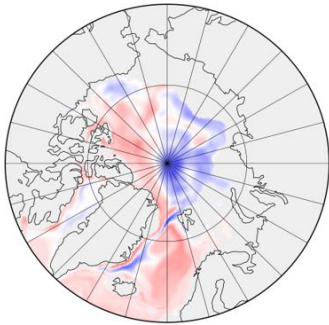
Figure 12: Maps showing the difference in stratification strength (ΔPE , MJ/m²) between 1x climate perturbation experiment (top row) and 2x climate change perturbation experiment (bottom row) for period 1 (1982-2001) (right hand side with zoom into Nordic Seas).

Both the 1x climate change perturbation and 2x climate change perturbation applied to period 1 lead to widespread intensification of stratification strength (Figure 12). An exception is the western Nordic Seas, Davis Strait and the Amundsen Basin.

dPE 2002-2021 - pert t2m+strd+tp fac1 anom

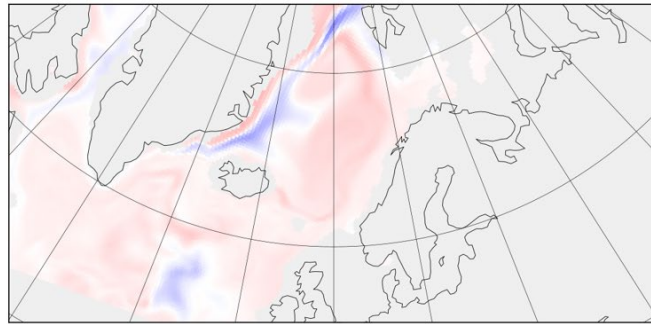


dPE (MJ/m2)
-0.05 -0.04 -0.03 -0.01 0.00 0.01 0.03 0.04 0.05
dPE 2002-2021 - pert t2m+strd+tp fac2 anom

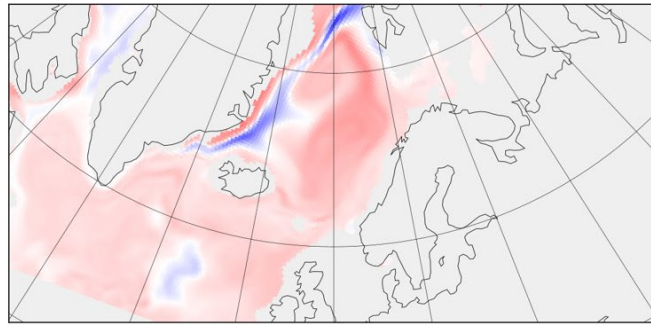


dPE (MJ/m2)
-0.05 -0.04 -0.03 -0.01 0.00 0.01 0.03 0.04 0.05

dPE 2002-2021 - pert t2m+strd+tp fac1 anom



dPE (MJ/m2)
-0.05 -0.04 -0.03 -0.01 0.00 0.01 0.03 0.04 0.05
dPE 2002-2021 - pert t2m+strd+tp fac2 anom



dPE (MJ/m2)
-0.05 -0.04 -0.03 -0.01 0.00 0.01 0.03 0.04 0.05

Figure 13: Maps showing the difference in stratification strength (ΔPE , MJ/m²) between 1x climate perturbation experiment (top row) and 2x climate change perturbation experiment (bottom row) for period 2 (2002-2021) (right hand side with zoom into Nordic Seas).

For both the 1x climate change perturbation and 2x climate change perturbation applied to period 2 also lead to widespread intensification of stratification strength (Figure 13) except in the western Nordic Seas, Eurasian Basin and Beaufort Sea. In the eastern Nordic Seas, the intensification of the stratification is more intense than for period 1.

2.4 Release scenarios

The release scenarios encompass continuous releases of 1 TBq/year (Experiments C1 - C15) and instantaneous releases of 1 PBq (Experiments I1 - I12) (Table 1). For each of these release scenarios, experiments were performed with a bottom release at the depth of the submarine and those with a whole column release, respectively. Releases are performed for two periods of 2 decades duration:

- Period 1: 1982-2001
- Period 2: 2002-2021

Each of those experiments has been performed with an unperturbed atmospheric forcing as a baseline, and the climate change scenarios as described in the following.

	List of experiments	Period	Release	Climatic perturbation	Mixing
1	Cfs-start-1982-opt5-3- Ans_kappa_h-cont	1982- 2001	Bottom, 1 PBq/yr, continuous	-	-
2	Cfs-start-1982-opt5-3- Ans_kappa_h- t2m_strd_tp_pert_fac1- cont	1982- 2001	Bottom, 1 PBq/yr, continuous	2m temperature, long-wave down and precipitation, instant	-
3	Cfs-start-1982-opt5-3- Ans_kappa_h- t2m_strd_tp_pert_fac2- cont	1982- 2001	Bottom, 1 PBq/yr, continuous	2 times 2m temperature, long-wave down and precipitation, instant	-
4	Cfs-start-2002-opt5-3- Ans_kappa_h- cont	2002- 2021	Bottom, 1 PBq/yr, continuous	-	-
5	Cfs-start-2002-opt5-3- Ans_kappa_h-t2m_pert_fac1- cont	2002- 2021	Bottom, 1 PBq/yr, continuous	2m temperature, instant	-
6	Cfs-start-2002-opt5-3- Ans_kappa_h- t2m_strd_pert_fac1-inst	2002- 2021	Bottom, 1 PBq/yr, continuous	2m temperature, long-wave down, instant	-
7	Cfs-start-2002-opt5-3- Ans_kappa_h- tp_pert_fac1_cont	2002- 2021	Bottom, 1 PBq/yr, continuous	Precipitation, instant	-
8	Cfs-start-2002-opt5-3- Ans_kappa_h- t2m_strd_tp_pert_fac1-cont	2002- 2021	Bottom, 1 PBq/yr, continuous	2m temperature, long-wave down and precipitation, instant	-
9	Cfs-start-2002-opt5-3- Ans_kappa_h- t2m_strd_tp_pert_fac2-cont	2002- 2021	Bottom, 1 PBq/yr, continuous	2 times 2m temperature, long-wave down and precipitation, instant	-
10	Cfs-start-1982-opt5-3- Ans_kappa_h-cont_column	1982- 2001	Whole column, 1 PBq/yr , continuous	-	-
11	Cfs-start-1982-opt5-3- Ans_kappa_h- t2m_strd_tp_pert_fac1- cont_column	1982- 2001	Whole column, 1 PBq/yr, continuous	2m temperature, long-wave down and precipitation, instant	-
12	Cfs-start-1982-opt5-3- Ans_kappa_h- t2m_strd_tp_pert_fac2- cont_column	1982- 2001	Whole column, 1 PBq/yr, continuous	2 times 2m temperature, long-wave down and precipitation, instant	-
13	Cfs-start-2002-opt5-3- Ans_kappa_h-cont_Column	2002- 2021	Whole column, 1 PBq/yr, continuous	-	-
14	Cfs-start-2002-opt5-3- Ans_kappa_h- t2m_strd_tp_pert_fac1- cont_column	2002- 2021	Whole column, 1 PBq/yr, continuous	2m temperature, long-wave down and precipitation, instant	-
15	Cfs-start-2002-opt5-3- Ans_kappa_h- t2m_strd_tp_pert_fac2- cont_column	2002- 2021	Whole column, 1 PBq/yr , continuous	2 times 2m temperature, long-wave down and precipitation, instant	-

Table 1: (a) Continuous release experiments

	List of experiments	Period	Release	Climatic perturbation	Mixing
1	Cfs-start-1982-opt5-3-Ans_kappa_h-inst	1982-2001	Bottom, 1 Bq, instant	-	-
2	Cfs-start-1982-opt5-3-Ans_kappa_h-t2m_strd_to_pert_fac1-inst	1982-2001	Bottom, 1 Bq, instant	2m temperature, long-wave down and precipitation, instant	-
3	Cfs-start-1982-opt5-3-Ans_kappa_h-t2m_strd_to_pert_fac2-inst	1982-2001	Bottom, 1 Bq, instant	2 times 2m temperature, long-wave down and precipitation, instant	-
4	Cfs-start-2002-opt5-3-Ans_kappa_h-inst	2002-2021	Bottom, 1 Bq, instant	-	-
5	Cfs-start-2002-opt5-3-Ans_kappa_h-t2m_strd_to_pert_fac1-inst	2002-2021	Bottom, 1 Bq, instant	2m temperature, long-wave down and precipitation, instant	-
6	Cfs-start-2002-opt5-3-Ans_kappa_h-t2m_strd_to_pert_fac2-inst	2002-2021	Bottom, 1 Bq, instant	2 times 2m temperature, long-wave down and precipitation, instant	-
7	Cfs-start-1982-opt5-3-Ans_kappa_h-inst_Column	1982-2001	Whole column, 1 Bq, instant	-	-
8	Cfs-start-1982-opt5-3-Ans_kappa_h-t2m_strd_to_pert_fac1-inst_column	1982-2001	Whole column, 1 Bq, instant	2m temperature, long-wave down and precipitation, instant	-
9	Cfs-start-1982-opt5-3-Ans_kappa_h-t2m_strd_to_pert_fac2-inst_column	1982-2001	Whole column, 1 Bq, instant	2 times 2m temperature, long-wave down and precipitation, instant	-
10	Cfs-start-2002-opt5-3-Ans_kappa_h-inst_Column	2002-2021	Whole column, 1 Bq, instant	-	-
11	Cfs-start-2002-opt5-3-Ans_kappa_h-t2m_strd_to_pert_fac1-inst_column	2002-2021	Whole column, 1 Bq, instant	2m temperature, long-wave down and precipitation, instant	-
12	Cfs-start-2002-opt5-3-Ans_kappa_h-t2m_strd_to_pert_fac2-inst_column	2002-2021	Whole column, 1 Bq, instant	2 times 2m temperature, long-wave down and precipitation, instant	-

Table 1: (b) Instantaneous release experiments.

2.5 Model description

The model experiments are performed with NAOSIM (North Atlantic-Arctic Ocean-Sea Ice Model), a regional, coupled sea ice-ocean model. It has been developed at the Alfred Wegener Institute for Polar and Marine Research (Köberle and Gerdes, 2003). It is derived from the Geophysical Fluid Dynamics Laboratory modular ocean model MOM-2 (Pacanowski, 1995) and a dynamic-thermodynamic sea ice model with a viscous-plastic rheology (Hibler, 1979). NAOSIM has been used for numerous studies on the dynamics of the Arctic Ocean and the Nordic Seas (e.g., Gerdes et al., 2003; Kauker et al., 2003; Karcher et al., 2003). It

has also been previously applied to studies of the dispersion of tracers (Brown et al., 2016; Gerdes et al., 2001, 2005; Karcher et al., 2004, 2012, 2017; Kauker et al., 2016; Smith et al., 2021). Here we use a version with 30 levels in the vertical, which are unevenly spaced. The surface levels have a thickness of 20 m. The model domain encompasses the Arctic Ocean, the Nordic Seas and the Northern Atlantic Ocean North of approximately 50°N. At the open Bering Strait receives a net volume inflow from the Pacific Ocean of 0.8 Sv. At the Southern boundary and in the Bering Strait, open boundary conditions have been implemented following Stevens (1991), thereby allowing the outflow of tracers and the radiation of waves. The initial hydrography in January 1948 is adopted from the PHC winter climatology (Steele et al., 2001), while a yearly mean climatology is used as a reference for surface salinity restoring on a time scale of 180 days. The restoring of sea surface salinity is a common method used to prevent the ocean salinity from drastically drifting away from the observed ocean state (Steele et al., 2001). Sea surface salinity restoring compensates for a mismatch between freshwater forcing data (e.g., precipitation and runoff) and model physics. In the absence of restoring the model drift is arbitrary, depending on the combination of forcing data set and model physics. The model is driven with daily atmospheric forcing from 1948 to 1979 (NCEP/NCAR reanalysis (Kalnay et al., 1996)) and continued to 1981 with CFS-R/v2 (Saha et al., 2010, 2011). From 1982 to 2021 two forcing datasets were used, a continuation with CFS-R/v2 and one with ERA5 (Hersbach et al., 2020).

2.6 Scenario experiments

2.6.1 Scenario experiments for continuous bottom release

A release of 1 TBq/year was initiated at the depth of the submarine (bottom release) for the period 1 from 1982 to 2001 and for period 2 from 2002 to 2021 with unperturbed forcing to establish the baseline for the climate change scenario experiments.

The baseline experiment was driven with standard mixing parameterization and unmodified atmospheric forcing from the CFS reanalysis (Figure 14 Baseline experiment)

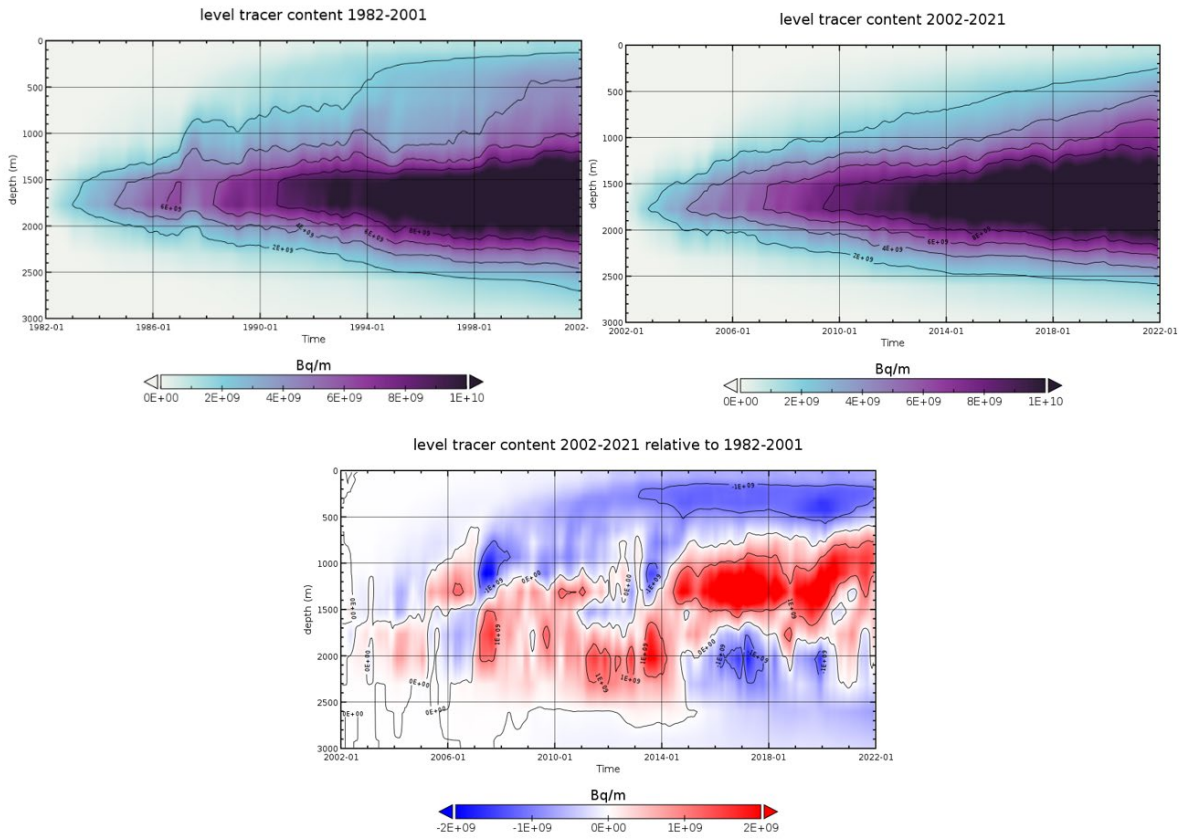


Figure 14: Baseline experiment - Continuous bottom release: Hovmoeller diagrams of the model domain mean tracer content versus depth (Bq/m) for the release period 1 1982-2001 (top left), period 2 2002-2021 (top right) and difference between period 2 and period 1 (bottom).

The difference in the dispersion between the two periods (Figure 14) reflects the combined effect of decadal variability and the long-term trends present in the atmospheric forcing. Period 1 (1982-2001) shows a much more intense vertical mixing compared to period 2 (2002-2021), reaching down to the depth of the submarine. The more intense mixing occurs sporadically and is due to deep reaching convection events occurring in period 1 (most prominently in 1987) that are almost absent in period 2 or at least much weaker. The mixing/convection events in period 1 in comparison to period 2 lead to an offset of the vertical distribution of the tracer once they occurred. In period 2 the top 500 m of the water column show lower concentrations of the tracer at the expense of the depth range 800-1500 m which exhibit higher concentrations

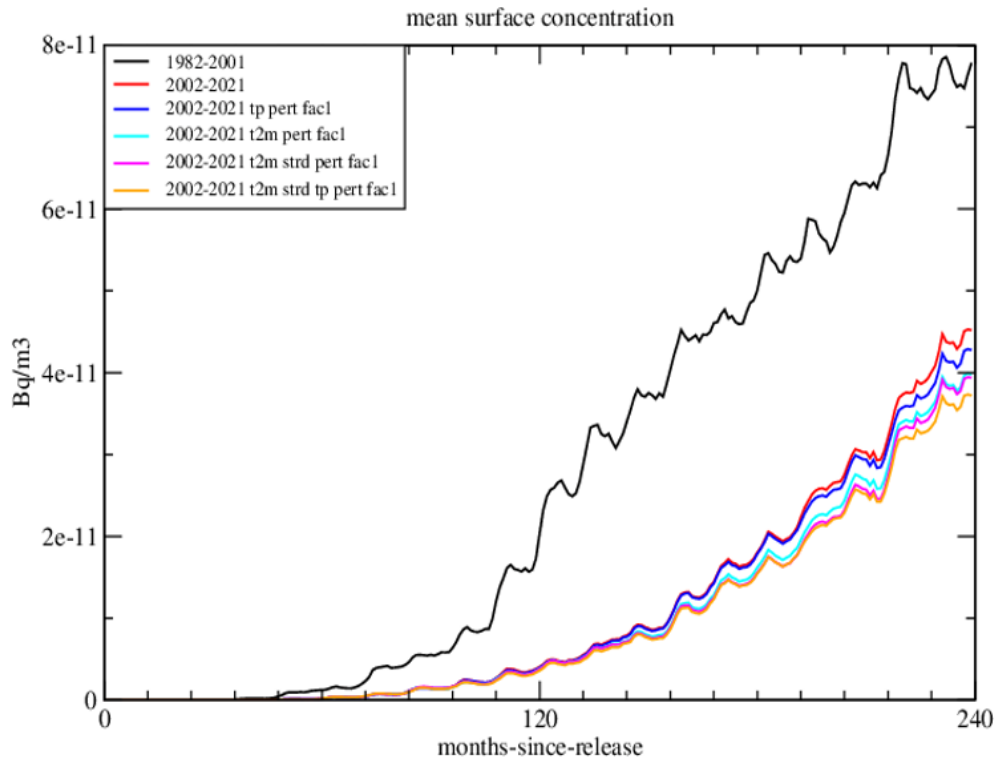


Figure 15: Graph of the mean surface layer concentration of tracer for 20 years in the model domain (monthly means). Continuous bottom release. Baseline simulation for period 1 (1982-2001, black) and period 2 (2002-2021, red) and climate change simulation with 1x climate change perturbations for single forcing parameters: precipitation (blue), 2m temperature (turquoise), and for combinations of perturbed forcing parameters: 2m temperature plus downward longwave radiation (magenta), 2m temperature plus downward longwave radiation plus precipitation (yellow).

The overall effect of the climate change induced perturbations for the surface layer tracer concentrations (model domain mean) is small in contrast to the decadal change between the two periods (Figure 15, red compared to black). The effect of 1x climate change perturbations has about the same size in terms of model domain mean surface tracer concentration for each of the perturbed variables: 2m temperature, downward longwave radiation and precipitation, respectively.

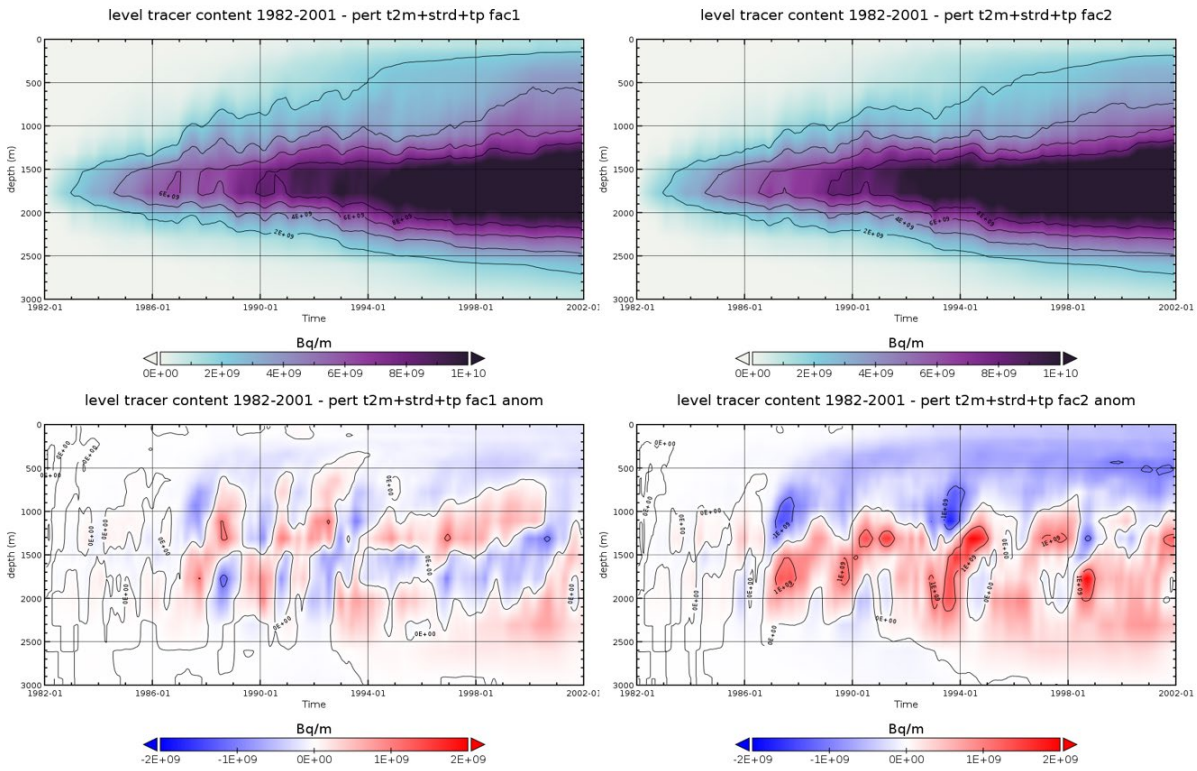


Figure 16: Climate change scenario experiments - Continuous bottom release for 1x perturbation (top left) and 2x perturbation (top right). Hovmoeller diagrams of the tracer content versus depth (model domain mean, Bq/m) for the release period 1 1982-2001 and the difference between scenario and unperturbed baseline experiment (bottom panels).

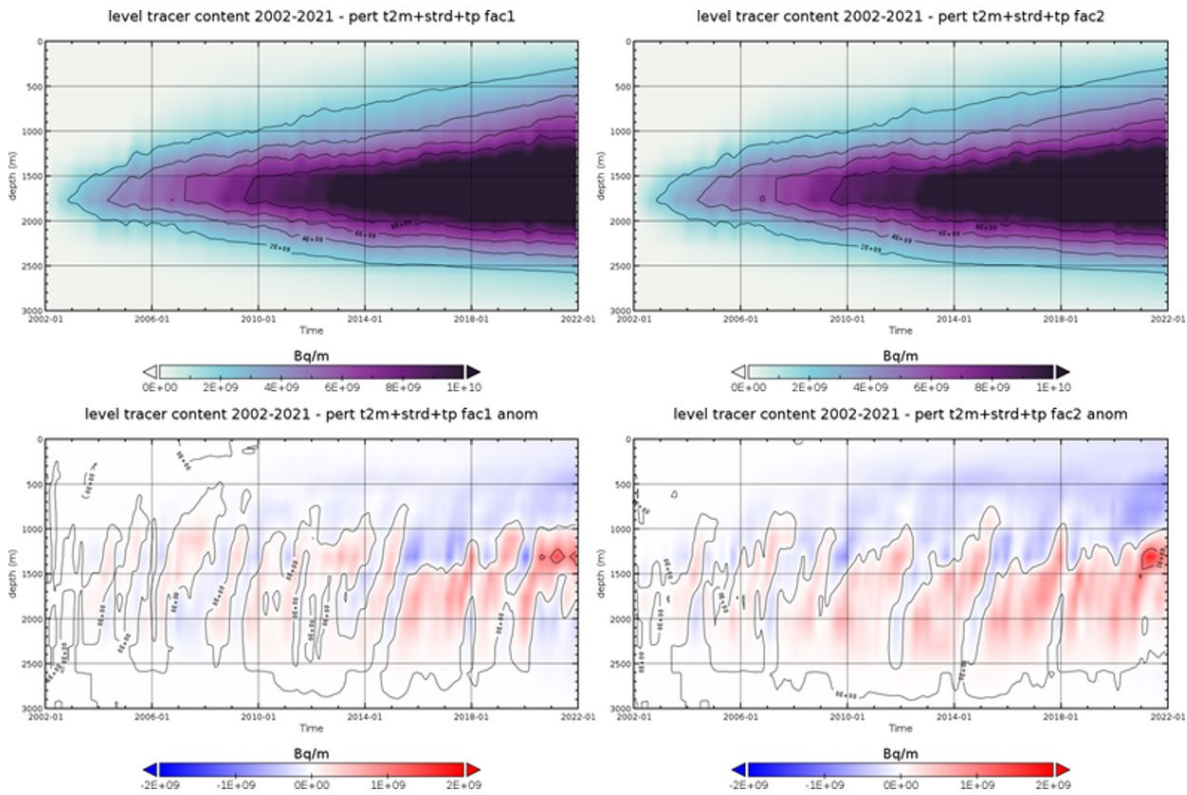


Figure 17: Climate change scenario experiments - Continuous bottom release for 1x perturbation (top left) and 2x perturbation (top right). Hovmoeller diagrams of the integrated tracer content versus depth in the

model domain (Bq/m) for the release period 2 2002-2021 and difference between scenario and unperturbed baseline experiment (bottom).

The combined climate change perturbations reduce the vertical exchange in the water column above the depth of the submarine for both periods. Imposing the 2x climate change perturbation increases the effect of a reduced vertical exchange considerably and leads to lower tracer content in the top 1000 m of the water column for both periods. The effect is very strong for the period 1 for which the more intense vertical mixing in the baseline (unperturbed) experiment is effectively diminished by the 2x climate change perturbation. The 2x climate change signal imposed on the surface forcing stabilizes the water column and stops almost all deep reaching convection events. But even for period 2 which had a lower vertical mixing in the unperturbed state, a 2x cli-mate change perturbation reduced the tracer content in the top 1000 m of the water column (Figure 17).

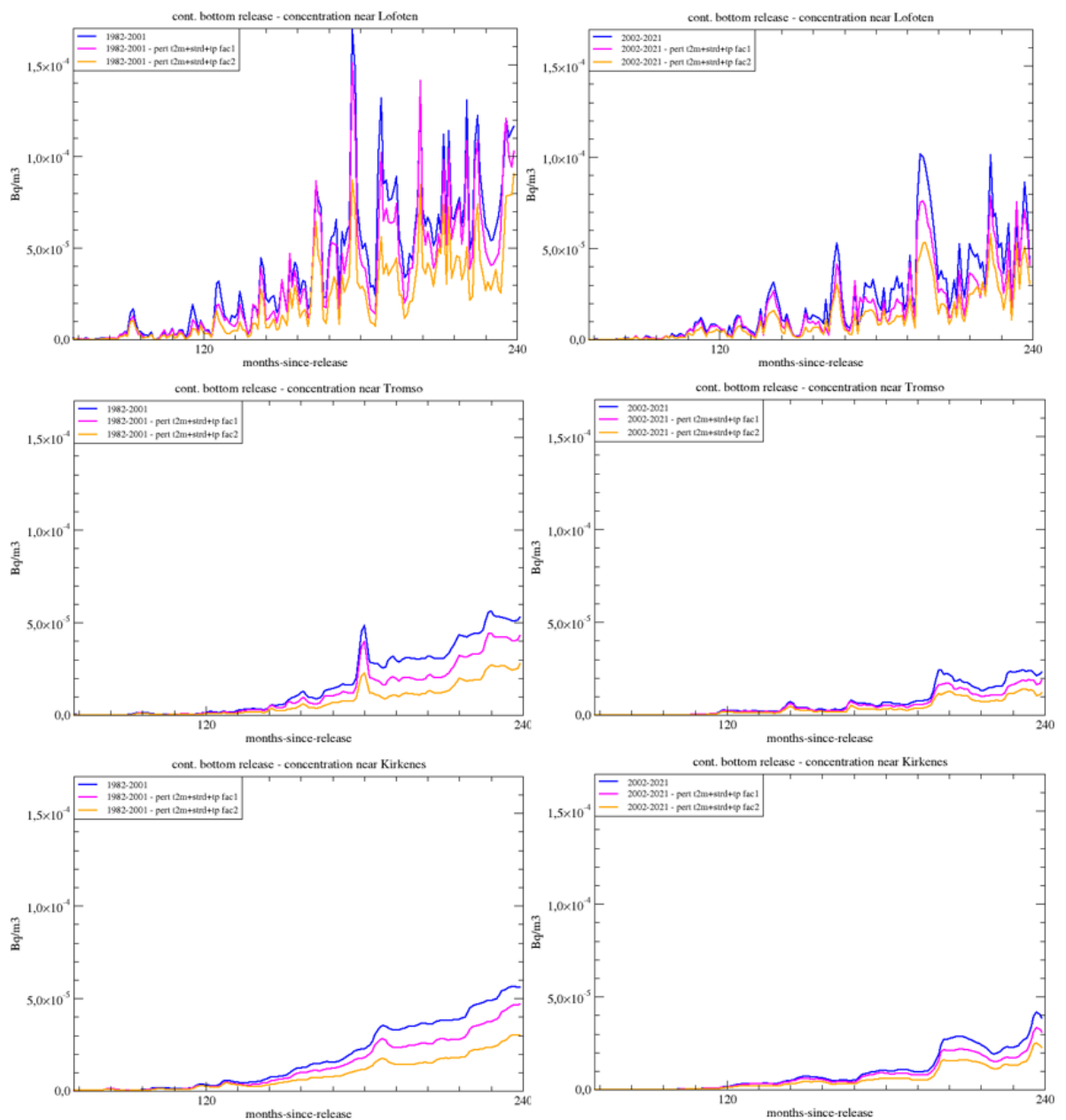


Figure 18: Continuous bottom release. Graphs of surface layer tracer concentration near Lofoten (top), Tromsø (middle) and Kirkenes (bottom) for period 1 (1982-2001, left) and period 2 (2002-2021, right).

Baseline simulation (blue), 1x climate change perturbation (magenta), 2x climate change perturbation (orange). Monthly means (solid).

We find a reduction of the surface concentrations in all three shown locations (Figure 18) for both periods in experiments with 1x and 2x climate change perturbations.

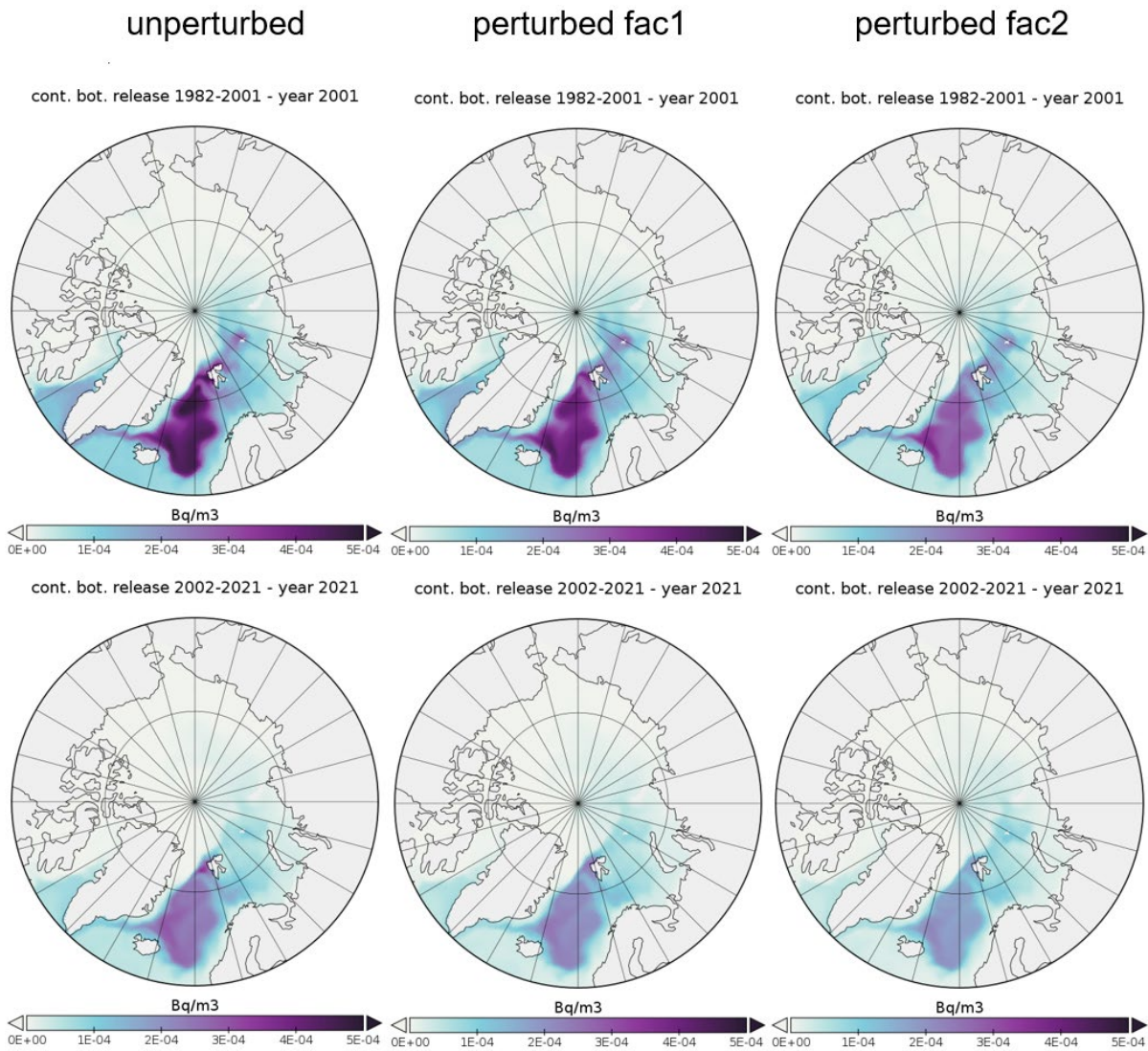


Figure 19: Continuous bottom release. Maps of surface layer tracer concentration 20 years after start in period 1 (1982-2001, top row) and period 2 (2002-2021, bottom row). Baseline simulation (left), 1x climate change perturbation (middle), 2x climate change perturbation (right).

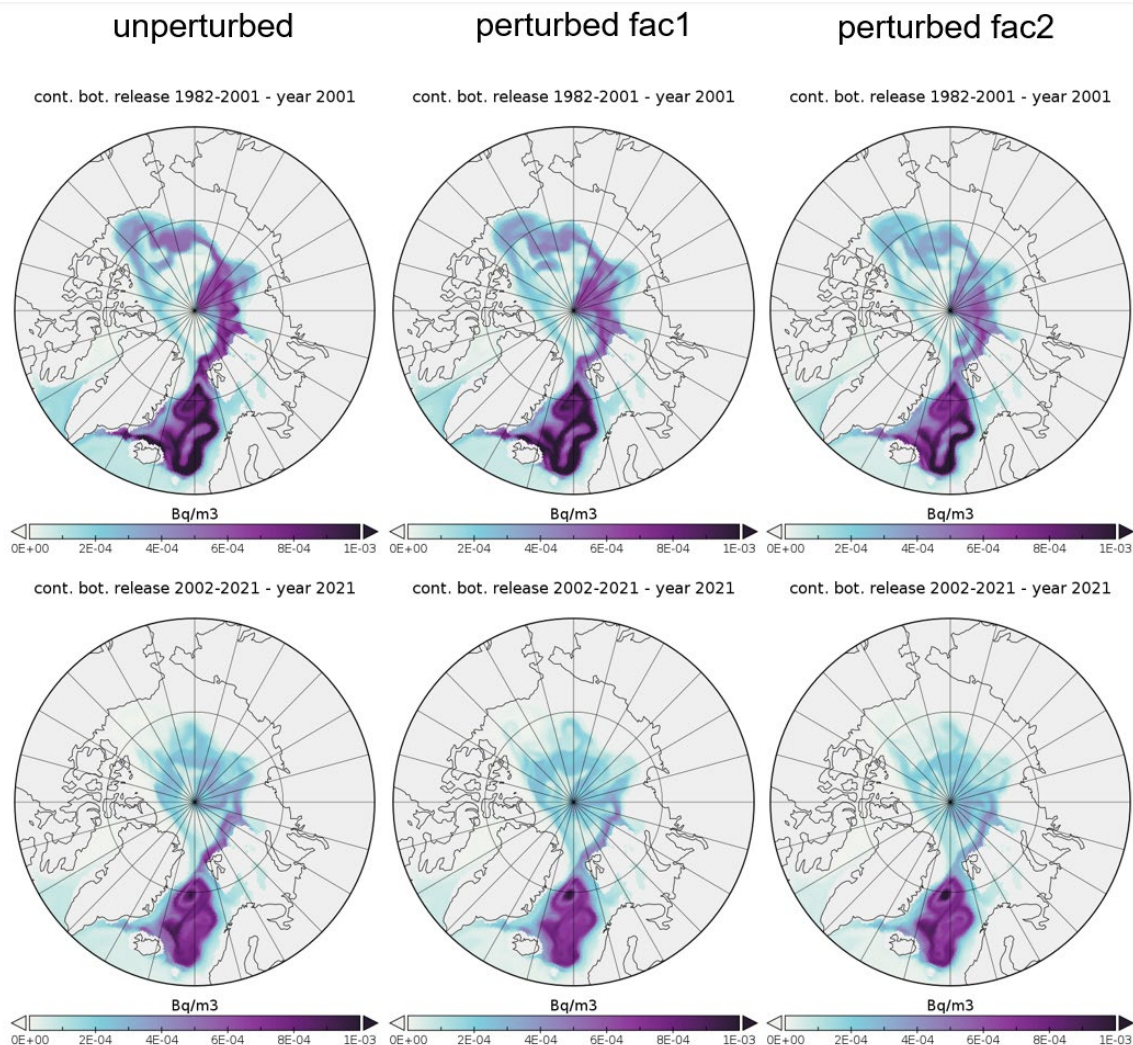


Figure 20: Continuous bottom release. Maps depicting 300m tracer concentration 20 years after start in period 1 (1982-2001, top row) and period 2 (2002-2021, bottom row). Baseline simulation (left), 1x climate change perturbation (middle), 2x climate change perturbation (right).

Maps of surface concentrations for year 20 after start of release for the unperturbed baseline experiment and both climate change perturbations show the previously found reduction of the surface concentration in climate change scenarios is widespread (Figure 19). The highest surface concentrations occur in western Nordic Sea, a recirculation of the contaminant with the offshore branch of NAC and outflow to Denmark Strait and Fram Strait, as well as a weak entry to Barents Sea take place. At 300m a strong intrusion to the Eurasian Basin of the Arctic and outflow through Denmark Strait take place. We find some reduction of concentrations in the climate change perturbation experiments, as less contaminant reaches 300m level from below (Figure 20).

2.6.2 Scenario experiments for continuous whole column release

The continuous release over the entire water column above the submarine is a very conservative worst-case scenario, as a fully mixed water column with continuous supply of tracer over a period of 20 years is not realistic. However, it can provide an insight into the dispersion characteristics for a continuously well mixed water close to the source.

A release of 1 TBq/year was initiated in the water column above the submarine (whole column release) for the period 1 from 1982 to 2001 and period 2 from 2002 to 2021 to establish the baseline for the climate change scenario experiments. The baseline experiment was driven with standard mixing parameterization and unmodified atmospheric forcing from the CFS reanalysis (Figure 21 Baseline experiments).

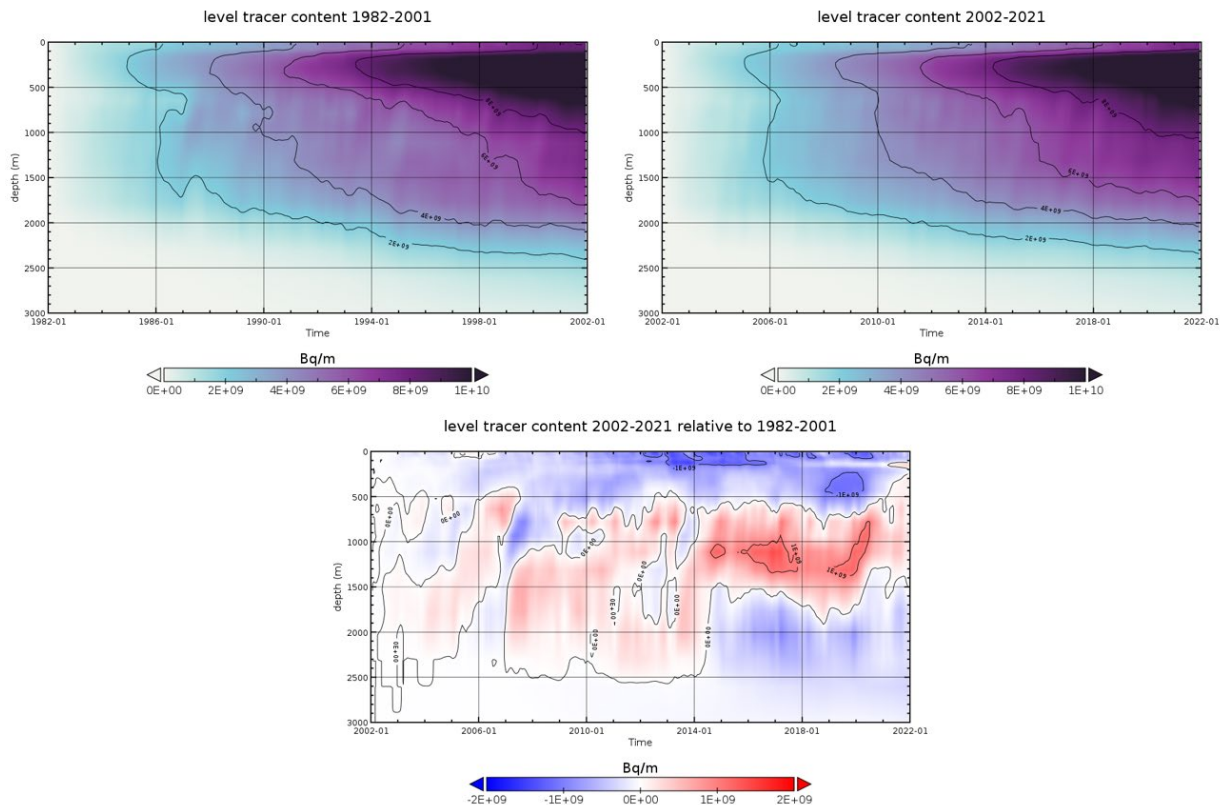


Figure 21: Baseline experiments - Continuous water column release: Hovmoeller diagrams of integrated tracer content versus depth in the model domain (Bq/m) for the release period 1 1982-2001 (top left), period 2 2002-2021 (top right) and difference between period 2 and period 1 (bottom).

For both periods the baseline experiment of release in the whole column shows an increase of the overall tracer content with time at all depths, but highest tracer content in the depth range of 200-1000m (Figure 21). This somewhat surprising result is due to a combination of higher advection speeds at the surface and down mixing of higher concentrations at the surface layer in regions away from the source location. As expected, the difference between the two periods reflects the lower vertical exchange in the top 500 m of the water column for period 2, leading to reduced tracer content there.

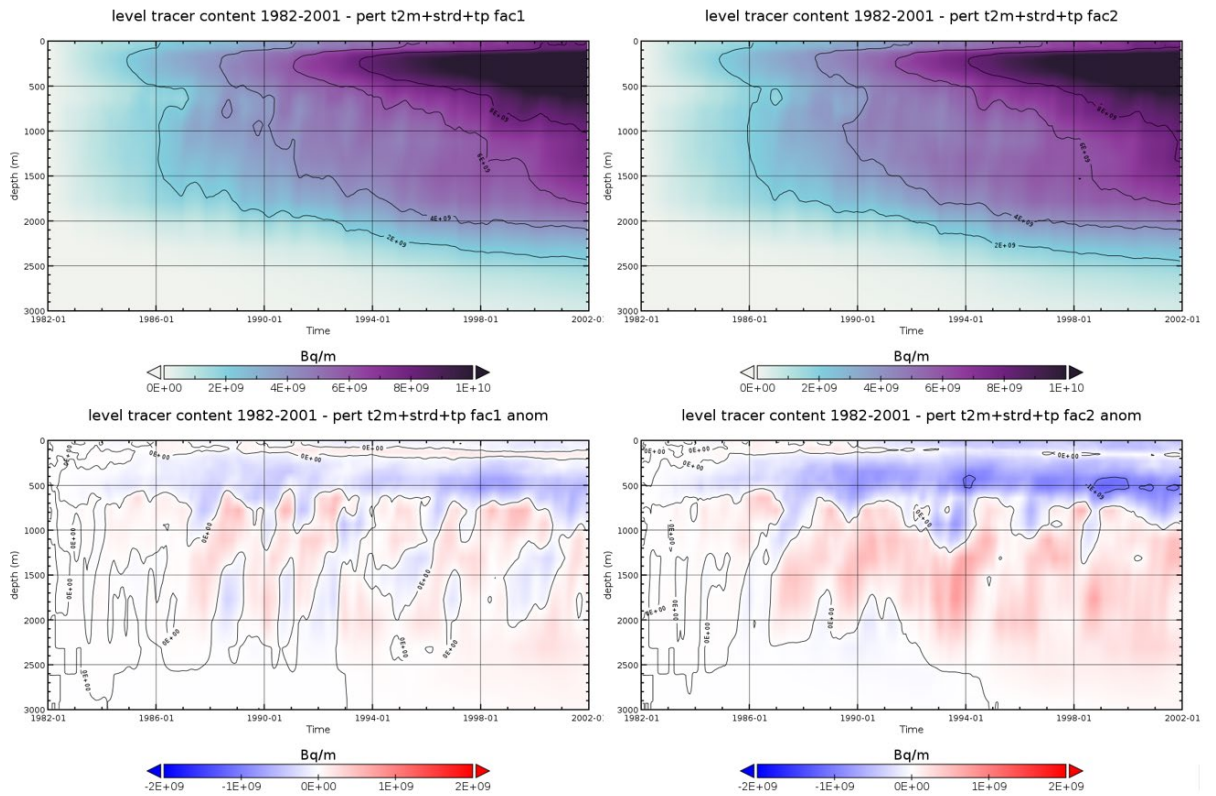


Figure 22: Climate change scenario experiments - Continuous water column release for 1x perturbation (top left) and 2x perturbation (top right). Hovmoeller diagrams of integrated tracer content versus depth in the model domain (Bq/m) for the release period 1 1982-2001 and difference between scenario and unperturbed baseline experiment (bottom).

Even though the release into the full column is continuous, the two climate change perturbation experiments show a reduction of the tracer content in the top 800 m (Figure 22) in period 1, reducing the tracer load being mixed upwards to the upper layers.

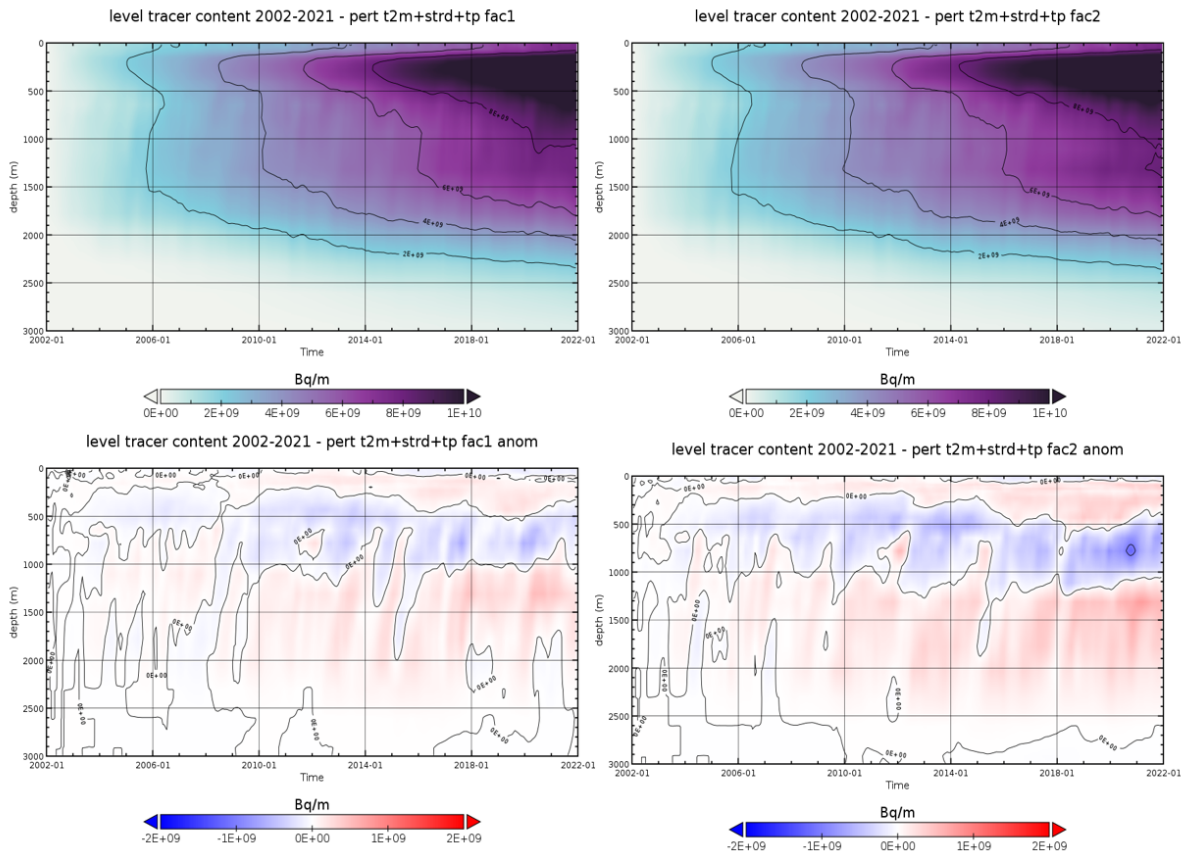


Figure 23: Climate change scenario experiments - Continuous water column release for 1x perturbation (top left) and 2x perturbation (top right). Hovmoeller diagrams of integrated tracer content versus depth in the model domain (Bq/m) for the release period 1 1982-2001 and difference between scenario and unperturbed baseline experiment (bottom).

Even though the release into the full column is continuous, the two climate change perturbation experiments show a reduction of the tracer content in the top 800 m (Figure 23) in period 1, reducing the tracer load being mixed upwards to the upper layers.

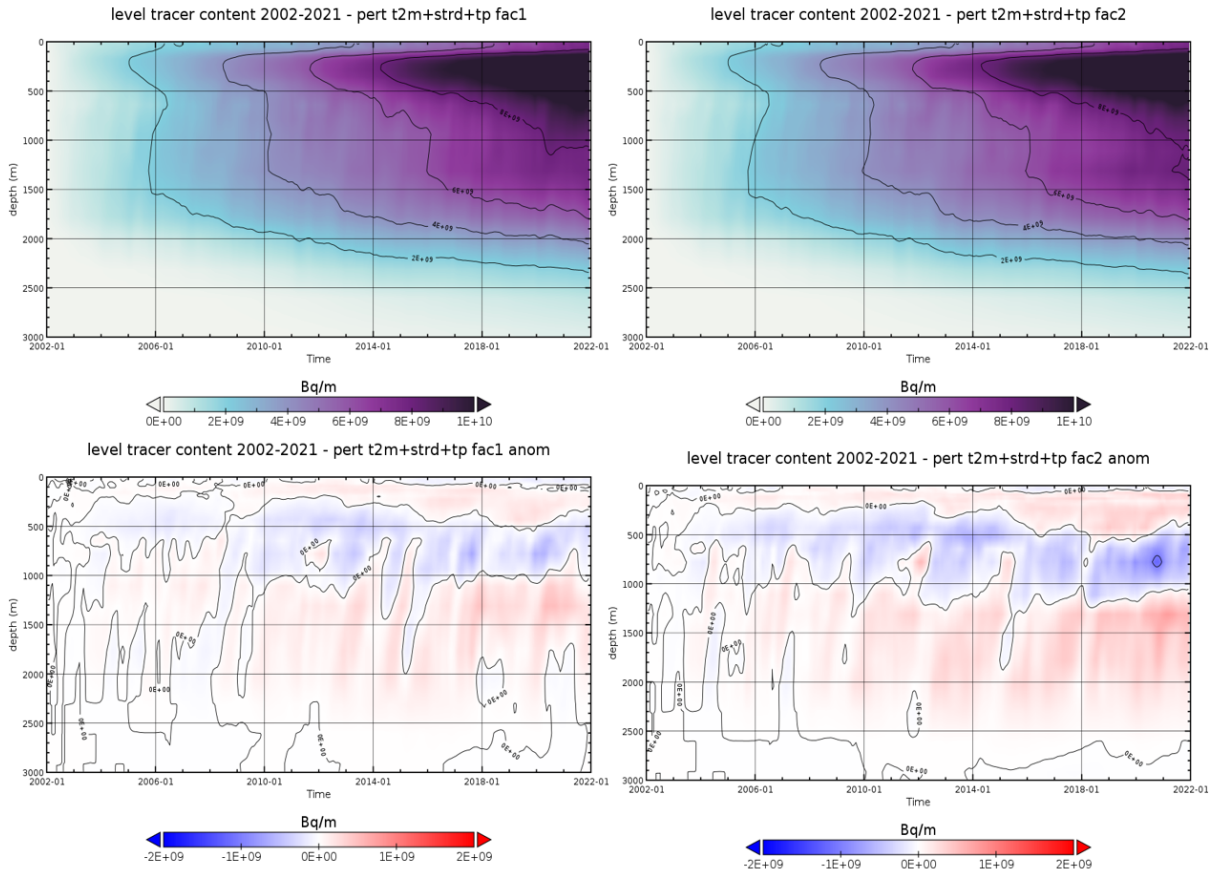


Figure 24: Climate change scenario experiments - Continuous water column release for 1x perturbation (top left) and 2x perturbation (top right). Hovmoeller diagrams of integrated tracer content versus depth in the model domain (Bq/m) for the release period 2 2002-2021 and difference between scenario and unperturbed baseline experiment (bottom).

In contrast to period 1, in period 2 the very surface layers of the top few hundred meters are experiencing a slightly enhanced tracer load in the case of the climate change perturbations, the layers below, down to about 1000m show a reduced load. (Figure 24).

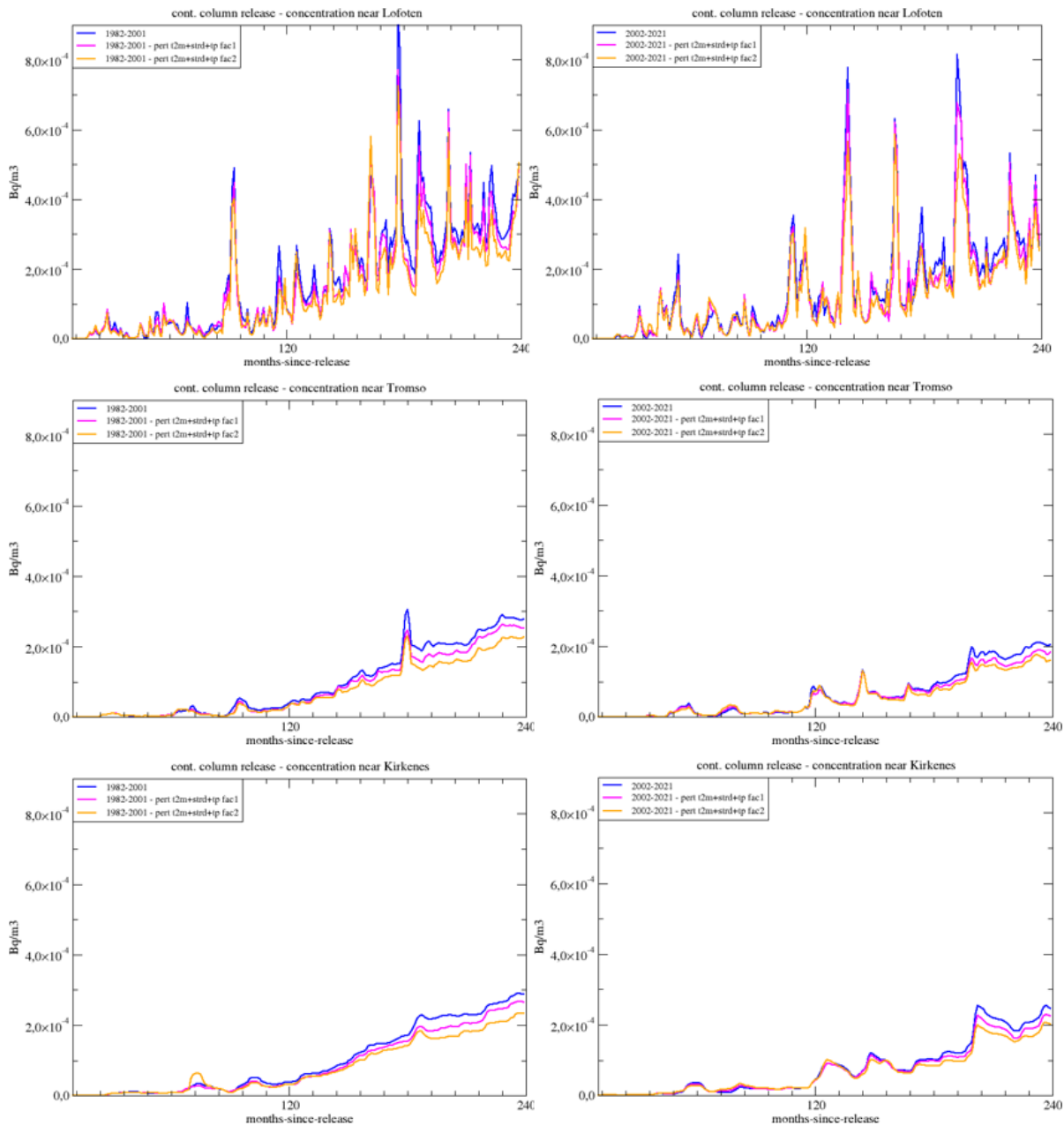


Figure 25: Continuous whole column release. Graphs of surface layer tracer concentration near Lofoten (top), Tromsø (middle) and Kirkenes (bottom) for period 1 (1982-2001, left) and period 2 (2002-2021, right). Baseline simulation (blue), 1x climate change perturbation (magenta), 2x climate change perturbation (orange) for period 1 (1982-2001, left) and period 2 (2002-2021, right). Monthly means (solid).

Surface concentrations at the selected locations are about one order of magnitude higher than for the continuous bottom release. Also, for this case the climate change experiments show slightly lower surface concentrations than the baseline simulation (Figure 25).

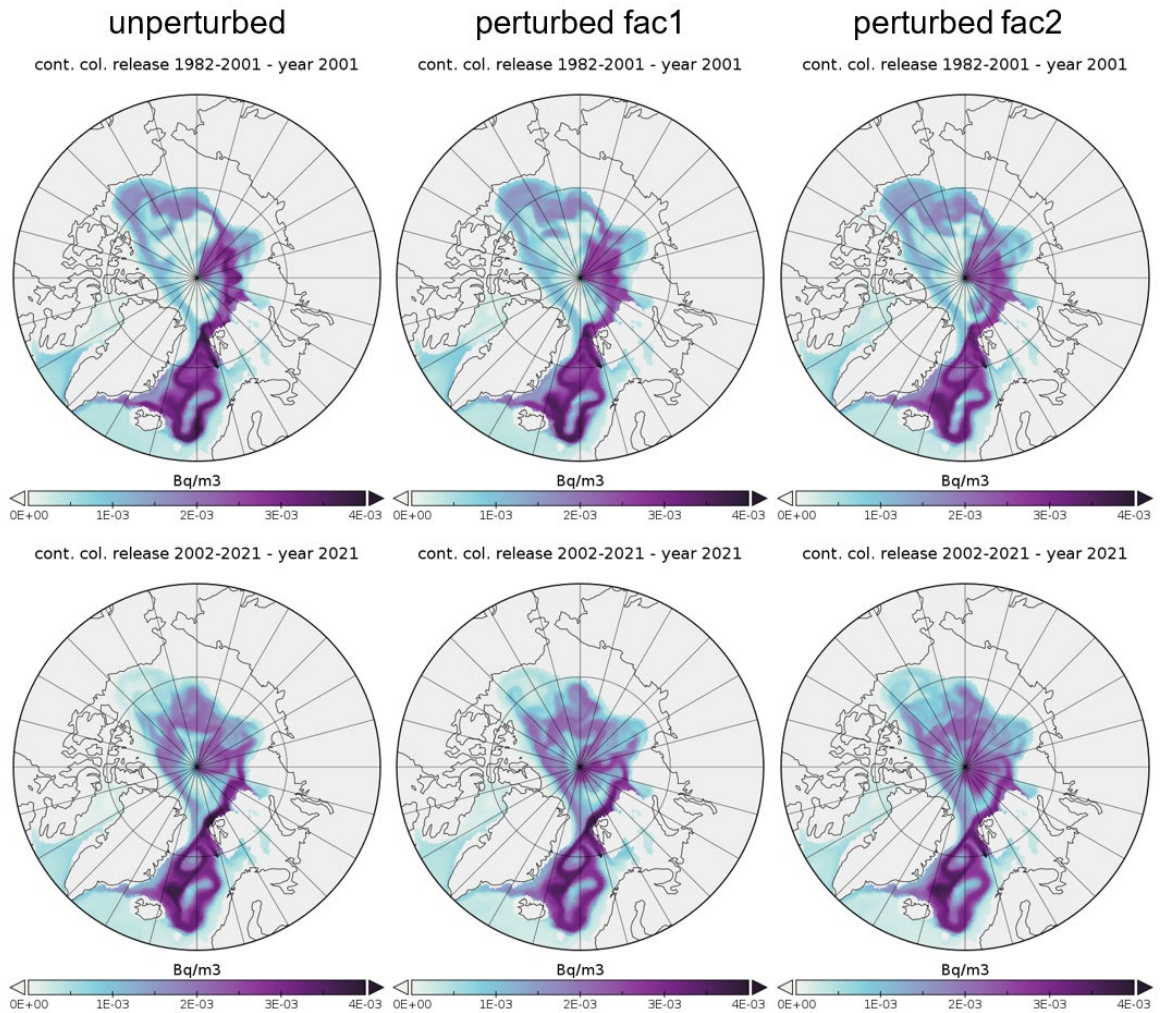


Figure 26: Continuous whole column release. Maps of 300m tracer concentration 20 years after start in period 1 (1982-2001, top row) and period 2 (2002-2021, bottom row). Baseline simulation (left), 1x climate change perturbation (middle), 2x climate change perturbation (right).

For the continuous whole column release, we find only a small impact of climate change perturbation on surface concentrations overall. The same holds for 300m water depth. Concentrations are slightly lower as compared to the baseline simulation (Figure 26).

2.6.3 Scenario experiments for instantaneous bottom release

An instantaneous release at the depth of the submarine is a scenario which evaluates a release of a large amount of radionuclide because of a sudden rupture. An instantaneous release of 1 PBq was initiated at the depth of the submarine (bottom release) for the period 1 from 1982 to 2001 and period 2 from 2002 to 2021 with unperturbed forcing to establish the baseline for the climate change scenario experiments.

The baseline experiment was driven with standard mixing parameterization and unmodified atmospheric forcing from the CFS reanalysis (Figure 27 Baseline experiments)

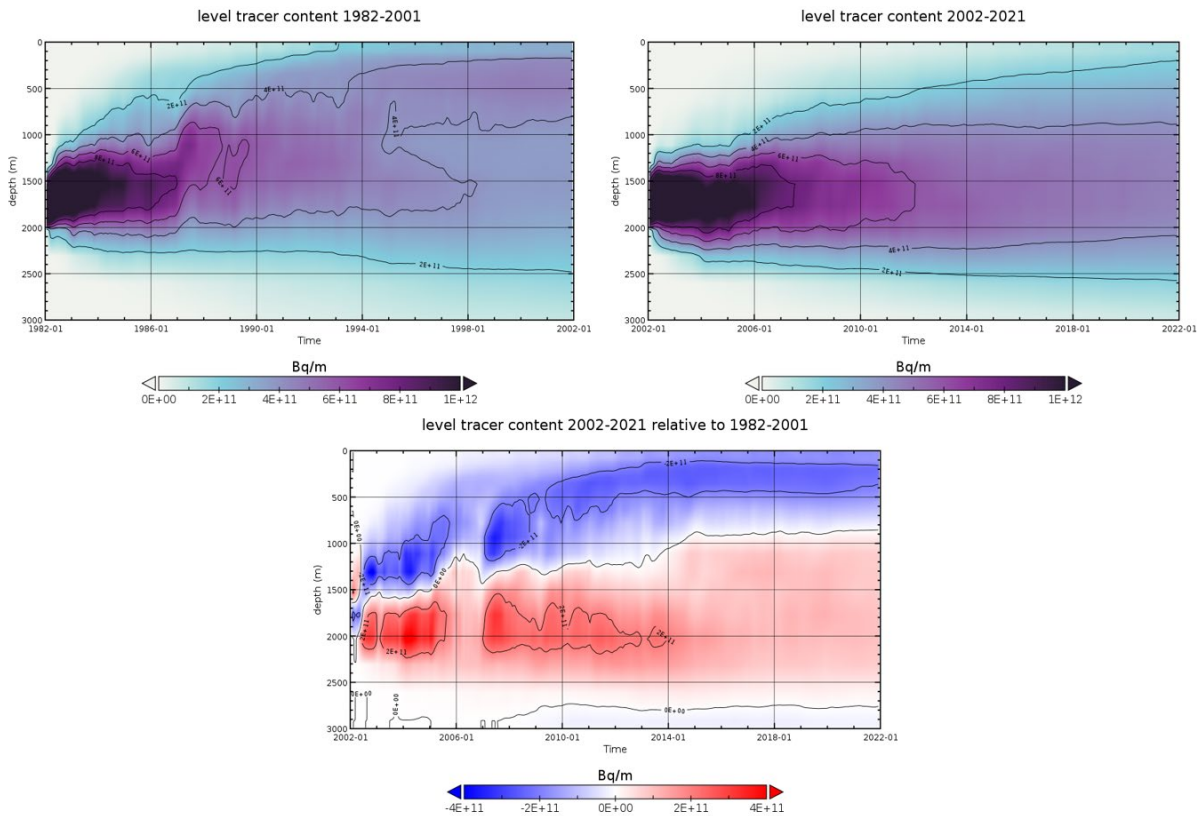


Figure 27: Baseline experiments - Instantaneous bottom release: Hovmoeller diagrams of integrated tracer content versus depth in the model domain (Bq/m) for the release period 1 1982-2001 (top left), period 2 2002-2021 (top right) and difference between period 2 and period 1 (bottom).

The consequence of an instantaneous bottom release from the submarine shows a strong difference between the two periods. The intense convection and mixing in the start of the period 1 leads to an early upward dispersion of the tracer. (Figure 27).

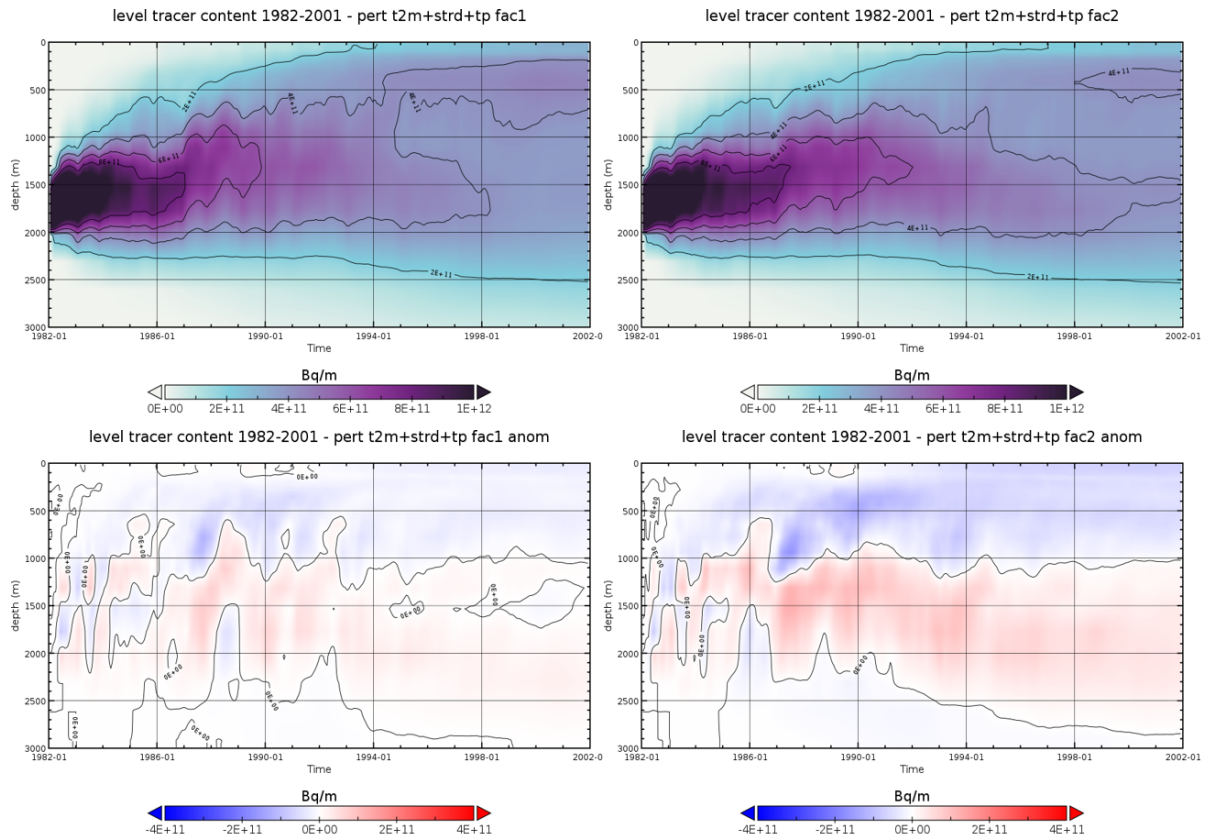


Figure 28: Climate change scenario experiments - Instantaneous bottom release for 1x perturbation (top left) and 2x perturbation (top right). Hovmoeller diagrams of integrated tracer content versus depth in the model domain (Bq/m) for the release period 2 1982-2001 and difference between scenario and unperturbed baseline experiment (bottom).

The climate change perturbation experiments for period 1 exhibit a reduction of the top 1000 m water column's tracer load for the entire 20 years in comparison to the baseline experiment. The reduction is stronger for the factor 2 perturbation (Figure 28) due to reduced convection.

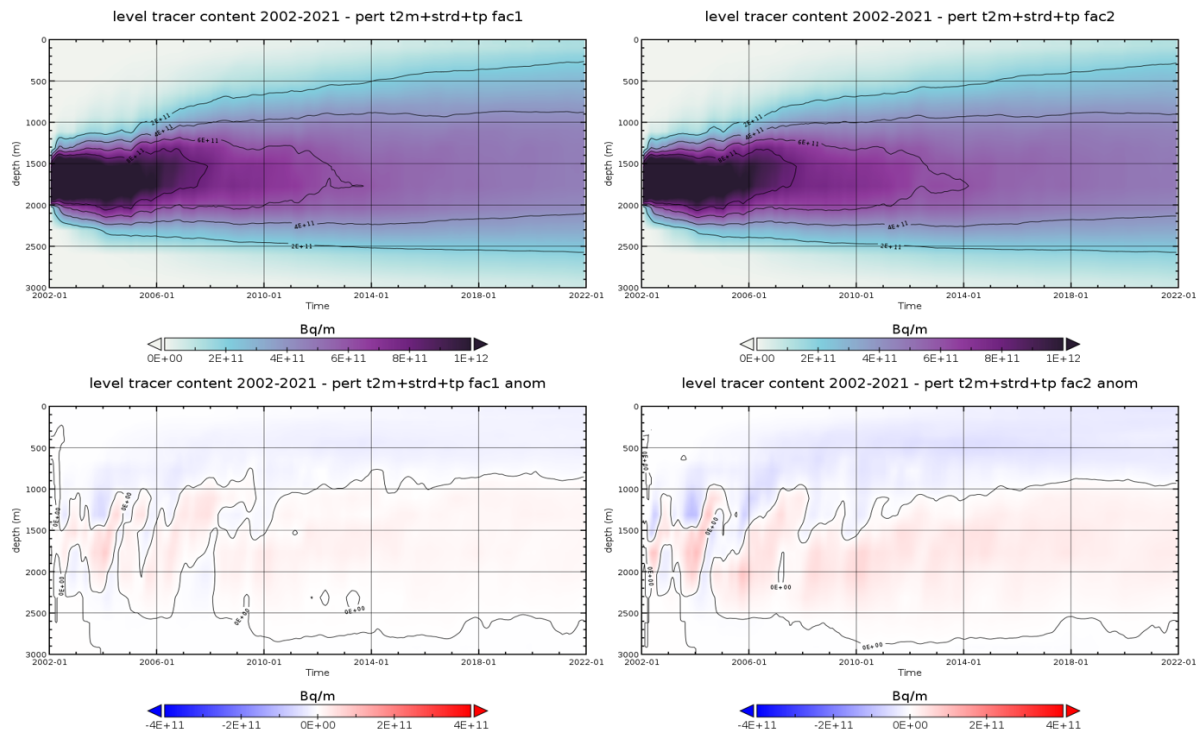


Figure 29: Climate change scenario experiments - Instantaneous bottom release for 1x perturbation (top left) and 2x perturbation (top right). Hovmoeller diagrams of integrated tracer content versus depth in the model domain (Bq/m) for the release period 1 2002-2021 and difference between scenario and unperturbed baseline experiment (bottom).

For period 2 we also find a reduction of the top 1000m tracer load in the domain relative to the baseline experiment. The reduction is slightly stronger for the factor 2 perturbation (Figure 29).

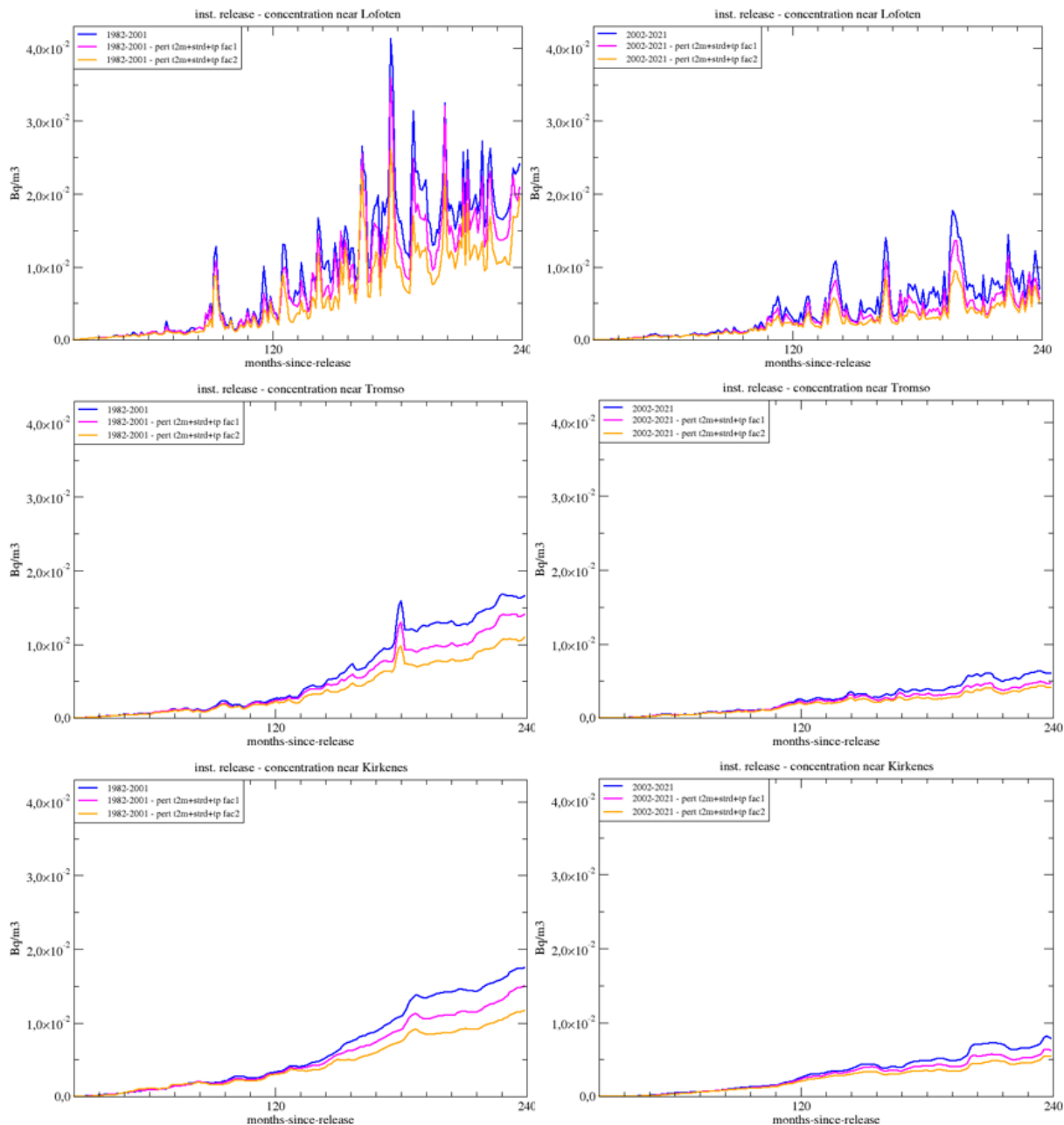


Figure 30: Instantaneous bottom release. Graphs of surface layer concentration near Lofoten (top), Tromsø (middle) and Kirkenes (bottom) for period 1 (1982-2001, left) and period 2 (2002-2021, right). Baseline simulation (blue), 1x climate change perturbation (magenta), 2x climate change perturbation (orange) for period 1 (1982-2001, left) and period 2 (2002-2021, right). Monthly means (solid).

Basic temporal behaviour in surface at the selected locations are not very different from continuous bottom release, but about 2 orders of magnitude higher concentrations are observed. Period 2 shows a much slower increase of local concentrations with time, reaching less than half the concentrations in the 20 years of simulation than in period 1 (Figure 30).

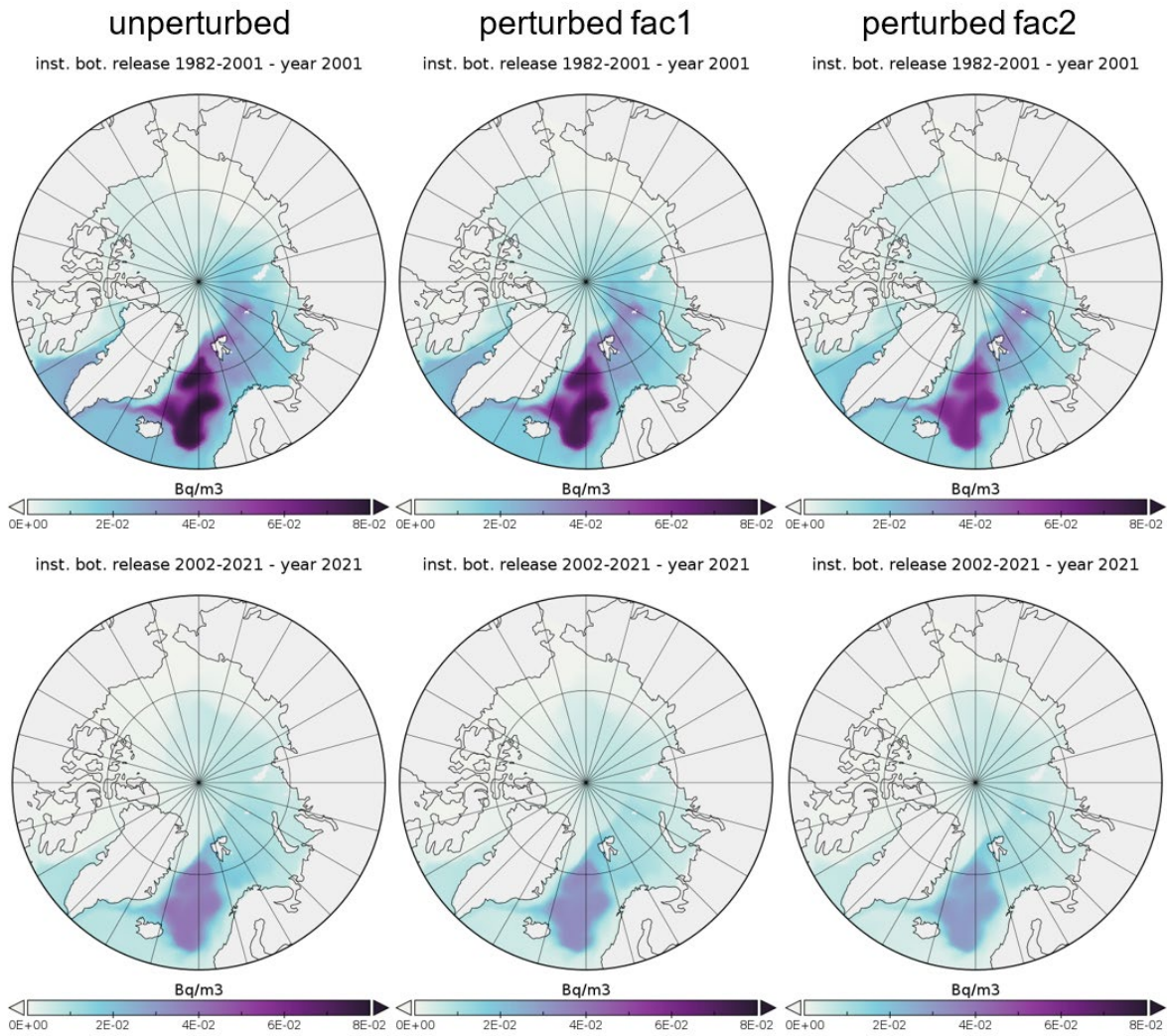


Figure 31: Instantaneous bottom release. Maps of surface layer tracer concentration 20 years after start in period 1 (1982-2001, top row) and period 2 (2002-2021, bottom row). Baseline simulation (left), 1x climate change perturbation (middle), 2x climate change perturbation (right).

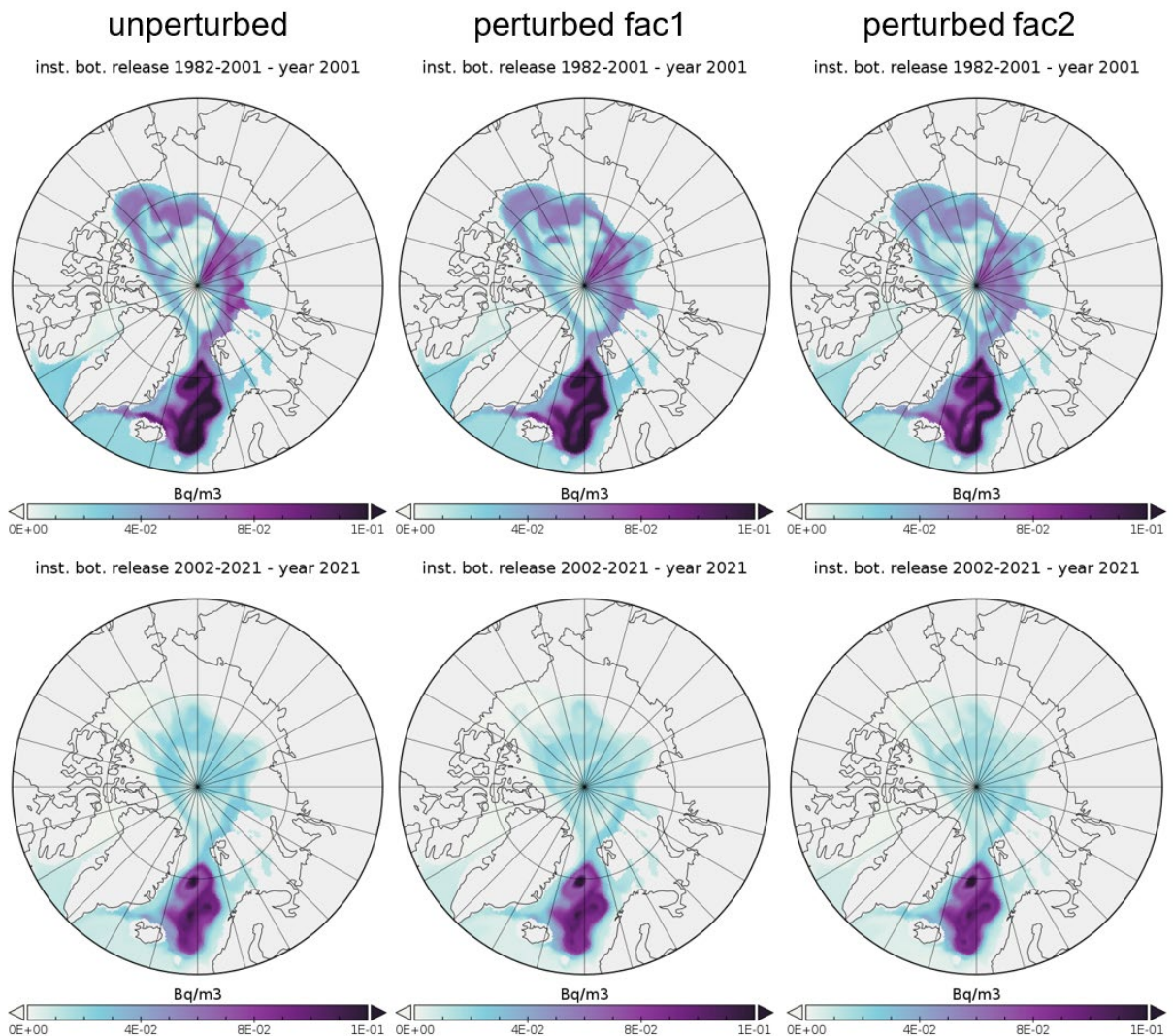


Figure 32: Instantaneous bottom release. Maps of 300m tracer concentration 20 years after start in period 1 (1982-2001, top row) and period 2 (2002-2021, bottom row). Baseline simulation (left), 1x climate change perturbation (middle), 2x climate change perturbation (right).

We find a slight reduction of surface concentrations in case of the climate change perturbations in contrast to the baseline experiments, period 2 again shows stronger reductions (Figure 31). There is smaller impact of climate change perturbation on concentrations at the 300 m level experiments than found at the surface (Figure 32).

2.6.4 Scenario experiments for instantaneous whole column release

An instantaneous release into the whole water column above the submarine is a scenario that might evolved during a saving operation under convection or strong vertical mixing conditions in the region. An instantaneous release of 1 PBq was initiated in the whole water column above the submarine (whole column release) for the period 1 from 1982 to 2001 and period 2 from 2002 to 2021 with unperturbed forcing to establish the baseline for the climate change scenario experiments.

The baseline experiment was driven with standard mixing parameterization and unmodified atmospheric forcing from the CFS reanalysis (Figure 33 Baseline experiments).

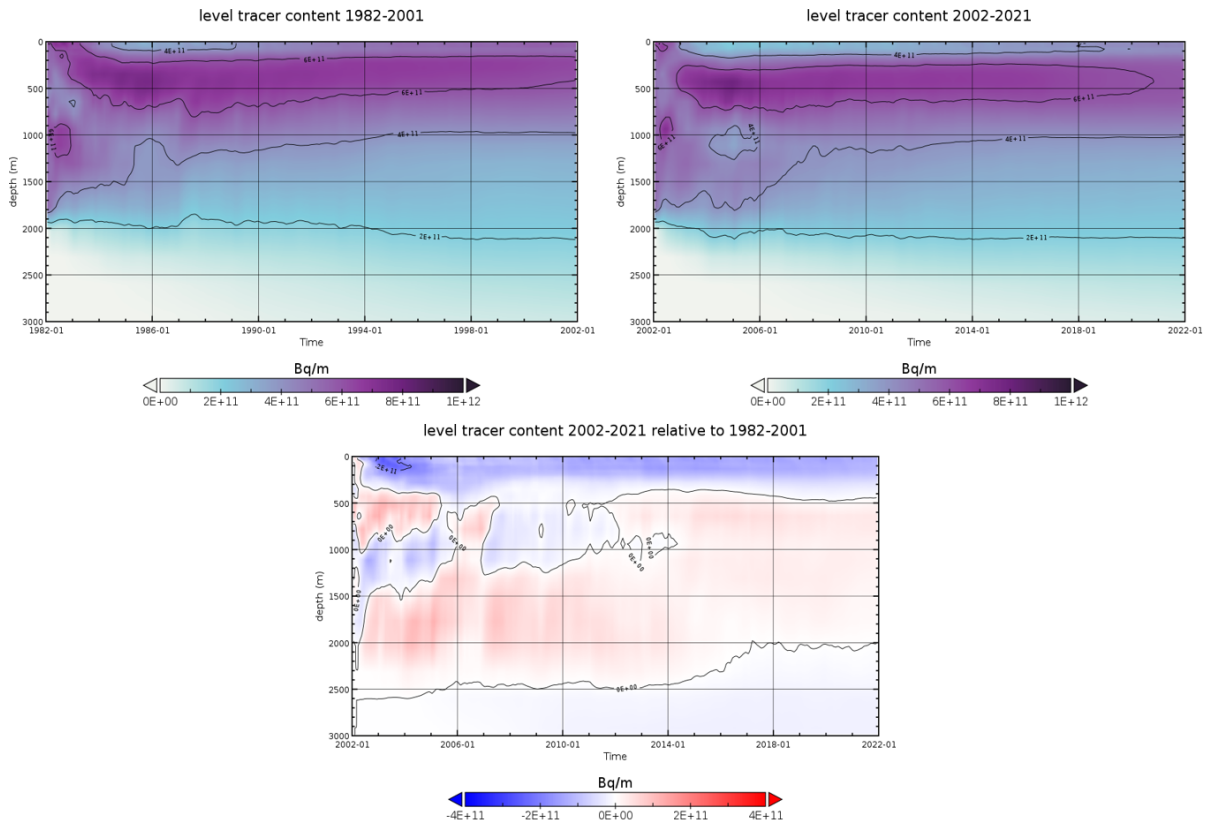


Figure 33: Baseline experiments - Instantaneous whole column release. Hovmoeller diagrams of integrated tracer content versus depth in the model domain (Bq/m) for the release period 1 1982-2001 (top left), period 2 2002-2021 (top right) and difference between period 2 and period 1 (bottom).

For an instantaneous release in the entire water column above the submarine there is a peak concentration developing at the 300 m level. The period 2 shows a stronger reduction of 0-500m tracer loads in the model domain in comparison to period 1 (Figure 33).

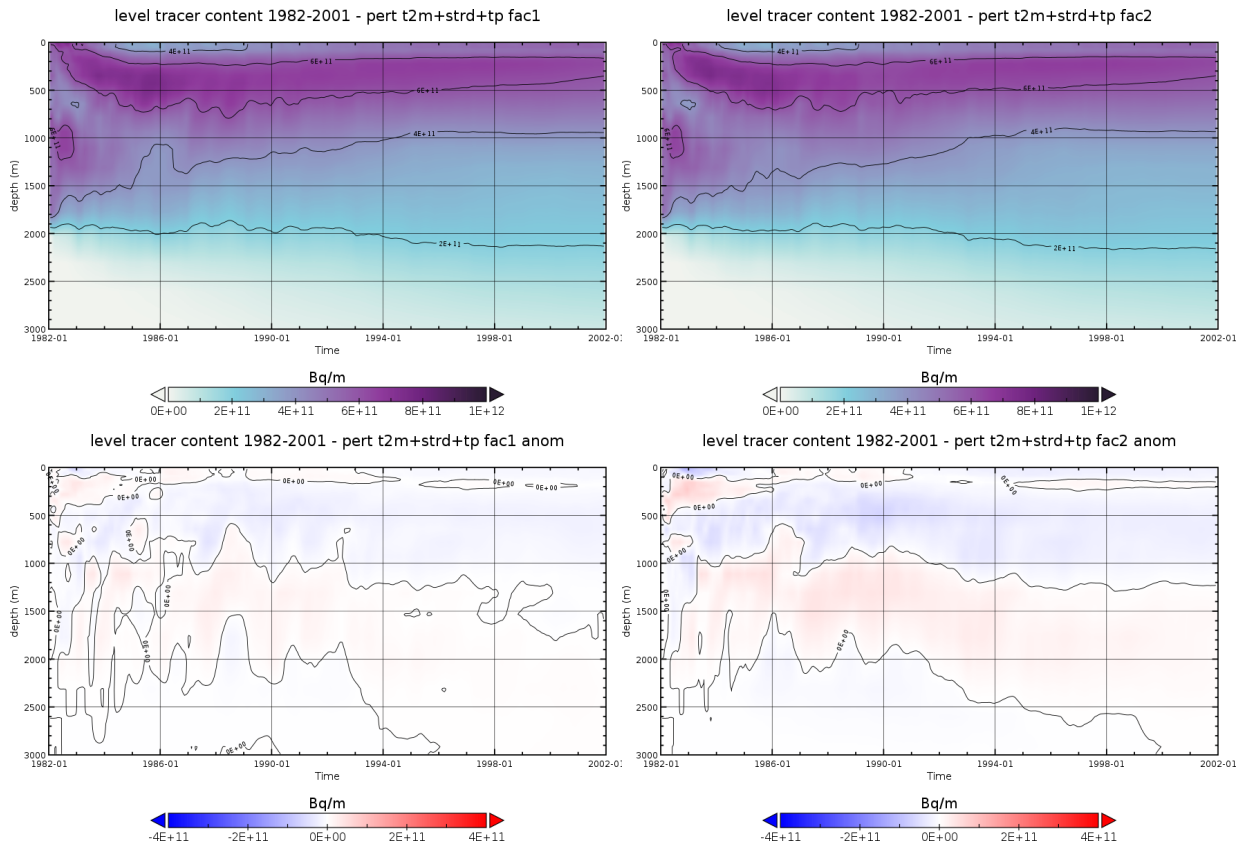


Figure 34: Climate change scenario experiments - Instantaneous whole column release for 1x perturbation (top left) and 2x perturbation (top right). Hovmoeller diagrams of integrated tracer content versus depth in the model domain (Bq/m) for the release period 1982-2001 and difference between scenario and unperturbed baseline experiment (bottom).

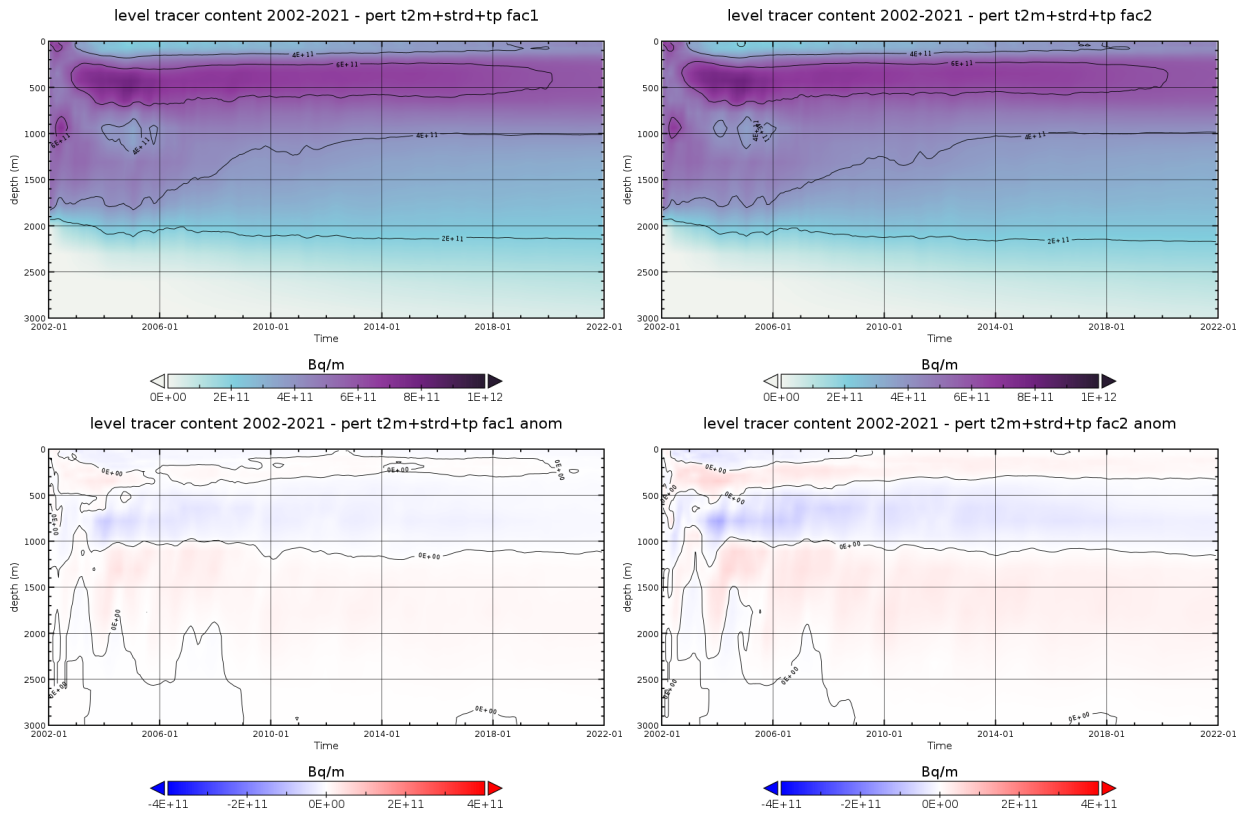


Figure 35: Climate change scenario experiments - Instantaneous whole column release for 1x perturbation (top left) and 2x perturbation (top right): Hovmoeller diagrams of integrated tracer content versus depth in the model domain (Bq/m) for the release period 2 2002-2021 and difference between scenario and unperturbed baseline experiment (bottom).

We find the peak tracer concentration developing at the 300 m level for both periods and both climate change perturbation scenarios as well. At intermediate levels between 200 and 1000 m depth the climate change experiments show reduced concentrations compared to the baseline experiments.

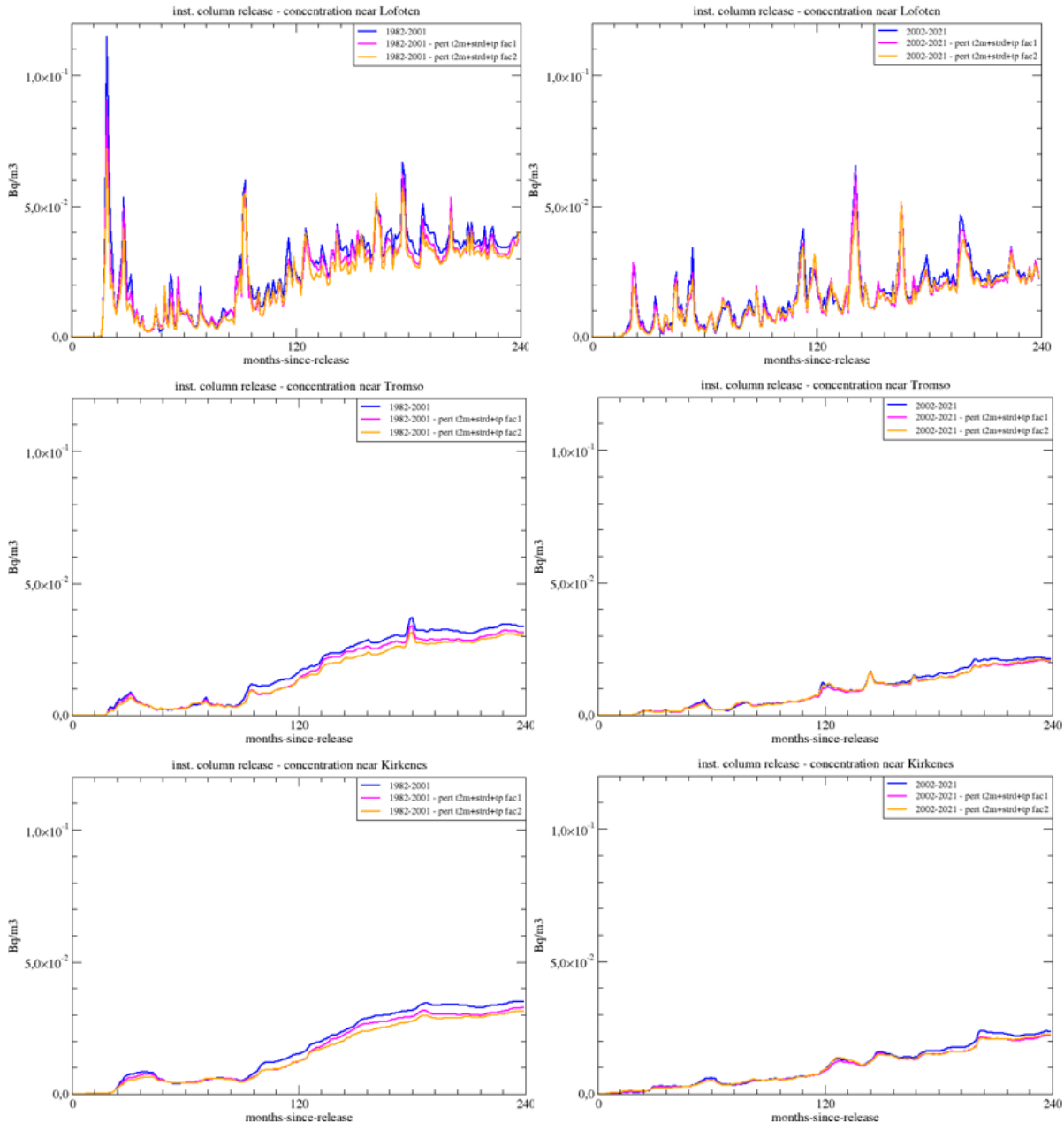


Figure 36: Instantaneous whole column release. Graphs of surface layer concentration near Lofoten (top), Tromsø (middle) and Kirkenes (bottom) for period 1 (1982-2001, left) and period 2 (2002-2021, right).

Baseline simulation (blue), 1x climate change perturbation (magenta), 2x climate change perturbation (orange) for period 1 (1982-2001, left) and period 2 (2002-2021, right). Monthly means (solid).

Little impact of climate change perturbation scenarios in case of whole column release (Figure 36).

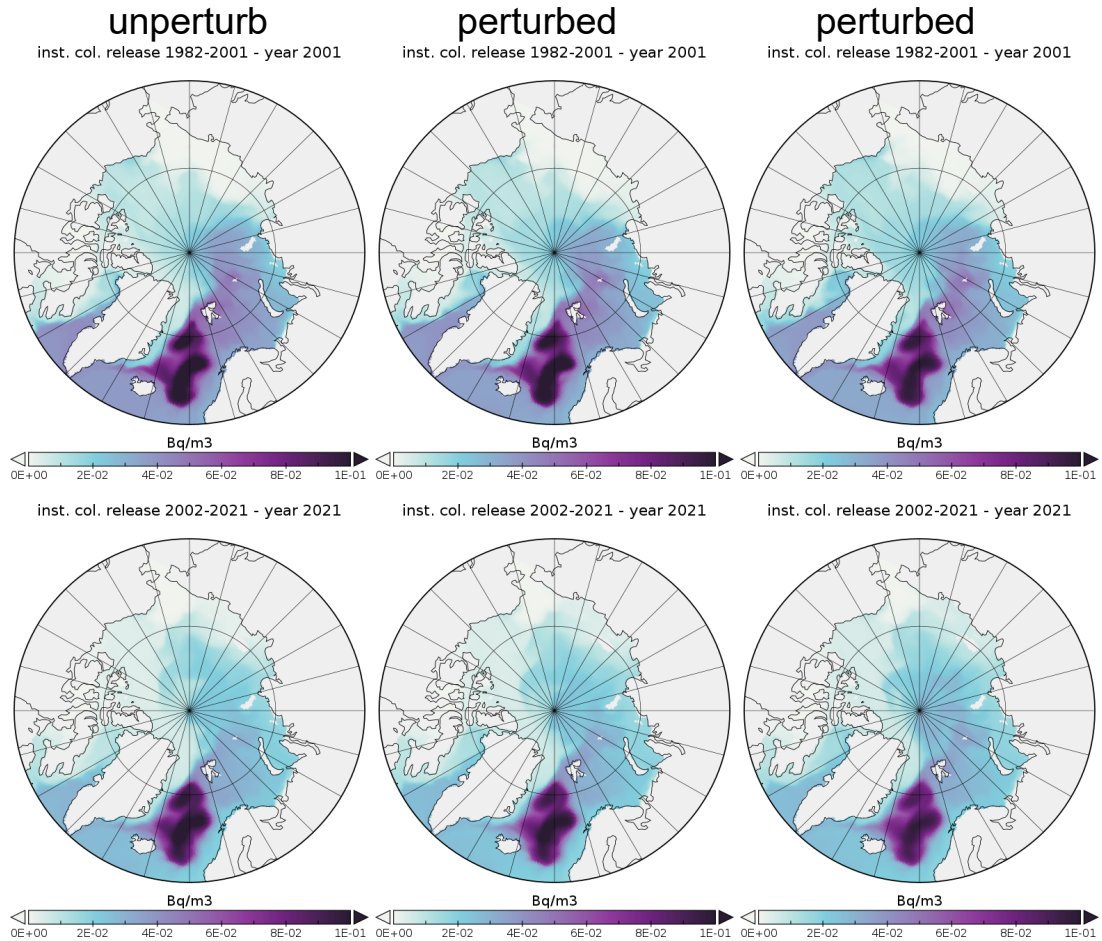


Figure 37: Instantaneous whole column release. Maps of surface layer tracer concentration 20 years after start in period 1 (1982-2001, top row) and period 2 (2002-2021, bottom row). Baseline simulation (left), 1x climate change perturbation (middle), 2x climate change perturbation (right).

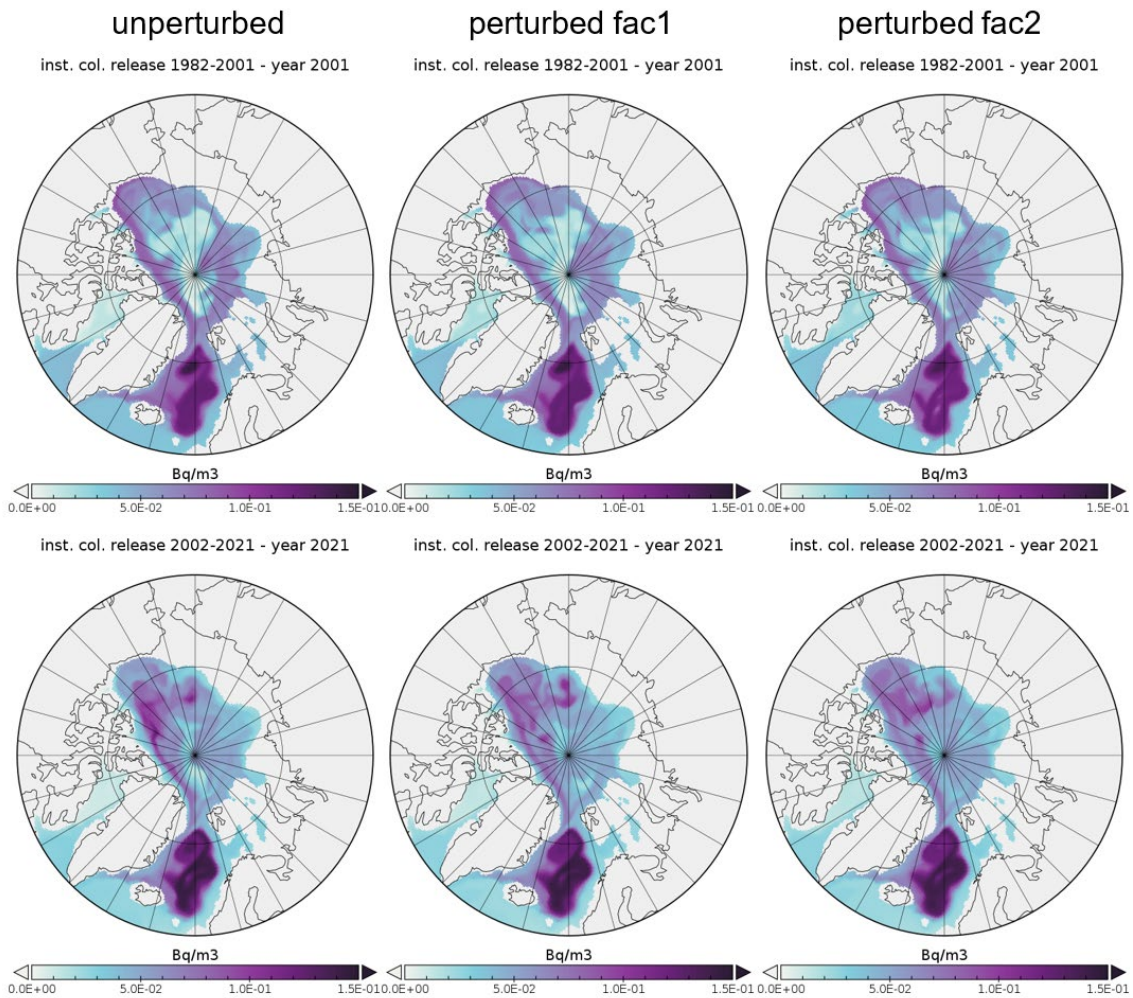


Figure 38: Instantaneous whole column release. Maps of 300m tracer concentration 20 years after start in period 1 (1982-2001, top row) and period 2 (2002-2021, bottom row). Baseline simulation (left), 1x climate change perturbation (middle), 2x climate change perturbation (right).

In the surface layer the bulk of the tracer after 20 years is still recirculating in the Nordic Seas, a light contamination of the Barents Sea and the northern North Atlantic occur (Figure 37). At 300m depth a widespread recirculation signal is found in the Arctic Ocean basin boundary current, in addition to highest concentration in the Nordic Seas (Figure 38).

3 Conclusions

Numerical dispersion experiments were made with hypothetical instantaneous (1PBq) and continuous (1TBq/y) release of a soluble radionuclide tracer from the submarine Komsomolets at the bottom of the Barents Sea slope in the Norwegian Sea. For both cases a bottom release and a whole water column release were performed, respectively.

Climate change scenarios were investigated, motivated by observed long term trends in the atmosphere over the past decades (1982-2021) which were identified in two atmospheric reanalysis data sets. The identified significant long-term trends in 2m temperature, longwave downward radiation, and precipitation in the high northern latitudes show increases in these variables. Then, the climate change scenario experiments were forced with a 1x and 2x climate change perturbation (the previously determined trends) added on the unperturbed forcing (= baseline experiments) for the periods 1982-2001 and 2002-2021.

In all climate change experiments reduced mixing and convection is obtained. The cause of the reduced mixing and convection is an intensified density contrast between the upper layer and deeper regions in the water column in the climate change scenarios, leading to a lower potential for deep water release to reach surface waters. Consequently, the climate change perturbation experiments show a reduced vertical mixing and convection in the Nordic Seas, thus reducing vertical mixing of the tracer, which leads to lower surface tracer concentrations and lower upper-level tracer content in comparison to the unperturbed baseline experiments.

Cases with a whole water column release (already well mixed tracer in the vertical at the location of the submarine) showed less sensitivity to climate change perturbations than the bottom release case.

The strongest impact of the climate change perturbations occurred for the period 1 (1982-2001) as this period showed more vertical mixing and convection in the unperturbed phase, and thus offered more potential for the suppression of mixing and convection.

The tracer concentrations for the selected locations in Kirkenes, Lofoten and Tromsø show an increasing trend over the 20 years of the experiments for all release and forcing scenarios, which means they did not reach equilibrium over the two decades.

The Lofoten location shows large fluctuations on seasonal and interannual time scale which is an indication of changes in the source waters reaching Lofoten on time, such as water from the high concentrations in the interior Nordic Seas to the west of Lofoten versus low concentrations in the Norwegian Coastal water arriving from the south. Highest local concentrations typically occur in autumn.

4 References

- AMAP 1998. AMAP assessment report: Arctic pollution issues. Arctic Monitoring and Assessment Programme (AMAP), Oslo, Norway. Xii+859 pp.
- Brakstad A., Våge K., Håvik L., Moore G.W.K. 2019. Water mass transformation in the Greenland Sea during the period 1986–2016, *J. Phys. Oceanogr.*, 49, 121-140, <https://doi.org/10.1175/JPO-D-17-0273.1>
- Brown, J., Hosseini, A. , Karcher, M. , Kauker, F. , Dowdall, M. , Schnur, R. and Strand, P. (2016): Derivation of risk indices and analysis of variability for the management of incidents involving the transport of nuclear materials in the Northern Seas , *Journal of Environmental Management*, 171 , pp. 195 203 .
<https://doi.org/10.1016/j.jenvman.2016.02.012>
- Gerdes R., Karcher M., Kauker F. and Koeberle C. 2001. Prediction for the spreading of radioactive substances from the sunken submarine "Kursk" in the Barents Sea. *EOS transactions, AGU*, 82(23): 253-257. <https://doi.org/10.1029/EO082i023p00253>
- Gerdes, R., Hurka, J., Karcher, M., Kauker, F., Koeberle, C. 2005. Simulated history of convection in the Greenland and Labrador seas 1948-2001, *AGU monograph Climate Variability of the Nordic Seas*, Bjerknæs Centre for Climate Research, Bergen, Norway, 221-238. <https://doi.org/10.1029/158GM15>
- Gladkov, G.A., Khlopkin, N.S., Lystsov, V.N., Neydanov, G.A., Pologikh, B.G., Sivintsev, Y.V. 1994. Assessment and prognosis of the state of nuclear installation of submarine 'Komsomolets'. Working group under leadership of Academician Khlopkin NS, RRC 'Kurchatov Institute', Moscow, Russia.
- Heldal, H.E, Gwynn, J., Teien, H-C., Volynkin, A., Kiel Jensen, L., Scheibener, S., Epifanov, A. 2019. Cruise report: Investigation of the marine environment around the nuclear submarine "Komsomolets" 6.-10. July 2019 (IMR cruise number 2019109), Havforskninginstituttet/ISSN 15036294/Nr. 9–2019.
https://www.hi.no/resources/Toktrapport-Komsomolets-ver_FINAL.pdf
- Hersbach, H., et al. 2020, The ERA5 global reanalysis, *Quarterly Journal of the Royal Meteorological Society*, 146, 730 <https://doi.org/10.1002/qj.3803>
- Hibler, W.D. III 1979. A dynamic thermodynamic sea ice model. *Journal of Physical Oceanography*, 9: 815-846. [https://doi.org/10.1175/1520-0485\(1979\)009%3C0815:ADTSIM%3E2.0.CO:2](https://doi.org/10.1175/1520-0485(1979)009%3C0815:ADTSIM%3E2.0.CO:2)
- Høibråten, S., Thoresen, P.E., Haugan, A. 1997. The sunken nuclear submarine Komsomolets and its effects on the environment, *Science of The Total Environment*, 202/1–3, 67-78, [https://doi.org/10.1016/S0048-9697\(97\)00105-8](https://doi.org/10.1016/S0048-9697(97)00105-8)
- Gwynn, J.P., Heldal, H.E., Flo, J.K., Sværen, I., Gäfvert, T., Haanes, H., Føyn, L., Rudjord, A.L. 2018. Norwegian monitoring (1990–2015) of the marine environment around the sunken nuclear submarine Komsomolets, *Journal of Environmental Radioactivity*, Volume 182, 2018, Pages 52-62,ISSN 0265-931X,
<https://doi.org/10.1016/j.jenvrad.2017.11.015>
- Kalnay, E., et al. (1996), The NCEP/NCAR 40-Year Reanalysis Project, *Bull. Am. Meteorol. Soc.*, 77, 437 – 495. [https://doi.org/10.1175/1520-0477\(1996\)077%3C0437:TNYRP%3E2.0.CO:2](https://doi.org/10.1175/1520-0477(1996)077%3C0437:TNYRP%3E2.0.CO:2)
- Karcher, M. , Hosseini, A. , Schnur, R. , Kauker, F. , Brown, J. , Dowdall, M. and Strand, P. (2017): Modelling dispersal of radioactive contaminants in Arctic waters as a result of potential recovery operations on the dumped submarine K 27 , *Marine Pollution Bulletin*, 116 (1 2), pp. 385 394 .
<https://doi.org/10.1016/j.marpolbul.2017.01.034>

- Karcher, M. J., Gerdes, R., Kauker, F., Koeberle, C. 2003. Arctic warming - Evolution and Spreading of the 1990s warm event in the Nordic Seas and the Arctic Ocean, *J. Geophys. Res.*, 108(C2), 3034.4
<https://doi.org/10.1029/2001JC001265>
- Karcher, M., Gerdes, R., Kauker, F. 2008. Long-term variability of Atlantic water inflow to the Northern Seas: insights from model experiments, *Arctic-Subarctic Ocean Fluxes: Defining the role of the Northern Seas in Climate*, Editors: B. Dickson, J. Meincke and P. Rhines, Springer. https://doi.org/10.1007/978-1-4020-6774-7_6
- Karcher, M., Gerdes, R., Kauker, F., Koeberle, C., and Yashayaev, I. 2005. Arctic Ocean change heralds North Atlantic freshening, *Geophys. Res. Lett.*, 32, L21606, <https://doi.org/10.1029/2005GL023861>
- Karcher, M., Smith, J. N., Kauker, F., Gerdes, R., & Smethie, W. M. 2012. Recent changes in Arctic Ocean circulation revealed by iodine-129 observations and modeling. *J. Geophys. Res. Oceans*, (1978–2012), 117(C8). <https://doi.org/10.1029/2011JC007513>
- Karcher, M., T. Hattermann, P. A. Dodd and T. T. Blæsterdalen, Comparison of Modeled Transports of Freshwater Fractions and Tracer-Derived Observations of Freshwater Fractions under various atmospheric conditions.. In prep.
- Karcher, M.J., S. Gerland, I. H. Harms, M. Iosjpe, H. E. Heldal, P. J. Kershaw and Sickel, M. 2004. The dispersion of ⁹⁹Tc in the Nordic Seas and the Arctic Ocean: a comparison of model results and observations, *J Environ Radioact*, 74(1-3): 185-198. <https://doi.org/10.1016/j.jenvrad.2004.01.026>
- Kauker, F., Kaminski, T. , Karcher, M. , Dowdall, M. , Brown, J. , Hosseini, A. and Strand, P. 2016. Model analysis of worst place scenarios for nuclear accidents in the Northern marine environment , *Environmental Modelling & Software*, 77 , pp. 13 18 . <https://doi.org/10.1016/j.envsoft.2015.11.021>
- Kauker, Frank, et al., 2003. Variability of Arctic and North Atlantic sea ice: a combined analysis of model results and observations from 1978 to 2001. *J. Geophys. Res. Oceans* (1978e2012) 108 (C6).
<https://doi.org/10.1029/2002JC001573>
- Kazenov, A., 2010. Technologies of radiation monitoring of dumped objects. In: IAEACEG Workshop on Removal of Spent Nuclear Fuel (SNF) and Radioactive Waste (RW) from Andreeva Bay, and Strategies for Handling Sunken Objects Containing SNF in the Arctic Ocean 24–26 February 2010, Hague, Netherlands.
- Köberle, C., and R. Gerdes. 2003, Mechanisms determining the variability of Arctic sea ice conditions and export, *J. Clim.*, 16: 2843–2858, doi:10.1175/1520-0442. <https://doi.org/10.1175/1520-0442>
- Liang, X., & Losch, M. 2018. On the effects of increased vertical mixing on the Arctic Ocean and sea ice, *Journal of Geophysical Research: Oceans*, 123, 9266–9282. <https://doi.org/10.1029/2018JC014303>
- Muilwijk, M., Nummelin, A., Heuzé, C., Polyakov, I. V., Zanowski, H., & Smedsrud, L. H. (2022). Divergence in climate model projections of future Arctic Atlantification. *Journal of Climate*, 1–53.
<https://doi.org/10.1175/JCLI-D-22-0349.1>
- Nejdanov, G., 1993. Cs-137 Contamination of Seawater Around the "Komsomolets" Nuclear Submarine, in: *Radioactivity and Environmental Security in the Oceans: New Research and Policy Priorities in the Arctic and North Atlantic*, June 7-9, 1993. Woods Hole Oceanographic Institution, Massachusetts, USA, pp. 119-133.

Nies, H., Harms, I.H., Karcher, M.J. et al. 1998. Anthropogenic radioactivity in the nordic seas and the arctic ocean — results of a joint project. Deutsche Hydrographische Zeitschrift 50, 313–343.

<https://doi.org/10.1007/BF02764228>

Nies, H., Harms, I.H., Karcher, M.J., Dethleff, D., Bahe, C. 1999. Anthropogenic radioactivity in the Arctic Ocean — review of the results from the joint German project, Science of The Total Environment, 237–238, 181-191, [https://doi.org/10.1016/S0048-9697\(99\)00134-5](https://doi.org/10.1016/S0048-9697(99)00134-5)

Pacanowski, R. C. (1995), MOM 2 Documentation, user's guide and reference manual, GFDL Ocean Group Tech. Rep. 3, Geophys. Fluid Dyn. Lab., Princeton Univ., Princeton, N. J..

Polyakov, I. V., et al., 2020. Borealization of the Arctic Ocean in Response Advection From Sub-Arctic Seas. Frontiers in Marine Science, 7, <https://doi.org/10.3389/fmars.2020.00491>

Saha, S., et al. 2010, The NCEP Climate Forecast System Reanalysis, BAMS, <https://doi.org/10.1175/2010BAMS3001.1>

Saha, S., et al. 2011, updated daily. NCEP Climate Forecast System Version 2 (CFSv2) 6-hourly Products. Research Data Archive at the National Center for Atmospheric Research, Computational and Information Systems Laboratory. <https://doi.org/10.5065/D61C1TXF>

Sivintsev Yu.V., Vakulovsky S.M., Vasiljev A.P., Vysotsky V.L., Gubin A.T., Danilyan V.A., Kobzev V.I., Kryshev I.I., Lavkovsky S.A., Mazokin V.A., Nikitin A.I., Petrov O.I., Pologikh B.G., Skorik, Yu.I., 2005. Technogenic Radionuclides in the seas Surrounding Russia. Radioecological Consequences of Radioactive waste Dumping in the Arctic and Far Eastern Seas (The White Book-2000), Moscow: IzdAt, 2005.

Smith, J. N., McLaughlin, F. A., Smethie, W. M. Jr., Moran, S. B., Lepore, K. 2011, Iodine-129, 137Cs, and CFC-11 tracer transit time distributions in the Arctic Ocean, J. Geophys. Res., 116, C04024, <https://doi.org/10.1029/2010JC006471>

Smith, J. N., Ellis, K. M., Kilius, L. R. 1998, ¹²⁹I and ¹³⁷Cs tracer measurements in the Arctic Ocean, Deep Sea Res., 45, 959–984, [https://doi.org/10.1016/S0967-0637\(97\)00107-6](https://doi.org/10.1016/S0967-0637(97)00107-6)

Smith, J. N., Ellis, K. M. and Boyd, T. M. 1999, Circulation features in the central Arctic Ocean revealed by nuclear fuel reprocessing tracers from SCICEX 95 and 96, J. Geophys. Res., 104, 29,663–29,677, <https://doi.org/10.1029/1999JC900244>

Smith, J. N., Karcher, M., Casacuberta, N., Williams, W. J., Kenna, T., & Smethie, W. M. 2021. A changing Arctic Ocean: How measured and modeled 129I distributions indicate fundamental shifts in circulation between 1994 and 2015. Journal of Geophysical Research: Oceans, 126, e2020JC016740. <https://doi.org/10.1029/2020JC016740>

Steele, M., Morley, R. Ermold, W. 2001, PHC: A global ocean hydrography with a high quality Arctic Ocean, J. Clim., 14: 2079 – 2087. [https://doi.org/10.1175/1520-0442\(2001\)014%3C2079:PAGOHW%3E2.0.CO;2](https://doi.org/10.1175/1520-0442(2001)014%3C2079:PAGOHW%3E2.0.CO;2)

Stevens, D.P. 1991. The Open Boundary Condition in the United Kingdom Fine-Resolution Antarctic Model. Journal of Physical Oceanography, 21 (9): 1494-1499. [http://dx.doi.org/10.1175/1520-0485\(1991\)021%3C1494:TOBCIT%3E2.0.CO;2](http://dx.doi.org/10.1175/1520-0485(1991)021%3C1494:TOBCIT%3E2.0.CO;2)

Vysotsky, V.L., Sivintsev, YuV., Sotnikov, V.A., Khokhlov, V.N., 2014. Release of manmade radionuclides into seawater from dumped and sunken nuclear- and radiation-hazardous objects. Therm. Eng. 61 (13), 931-945.

Yablokov, A.V., Karasev, V.K., Rumyantsev, V.M., Kokeev, M.E., Petrov, O.J., Lystsov, V.N., Emel'yanenkov, A.F., Rubtsov, P.M., 1993. Facts and Problems Related to Radioactive Waste Disposal in Seas Adjacent to the Territory of the Russian Federation. Small World Publishers Inc, Moscow, Russia.

Wu, Y., Stevens, Renfrew, D. P., I. A., & Zhai, X. (2021). The Response of the Nordic Seas to Wintertime Sea Ice Retreat, *Journal of Climate*, 34(15), 6041-6056. Retrieved Nov 28, 2022, from <https://journals.ametsoc.org/view/journals/clim/34/15/JCLI-D-20-0932.1.xml>

- 1 DSA-rapport 01-2024
Radioaktivitet i luft og strålingsnivå i omgivnadene 2024
- 2 DSA Report 02-2025
Ukrainian Regulatory Threat Assessment 2024
- 3 DSA Report 03-2025
Three Decades of UV-monitoring in Norway: Trends and Drivers
- 4 DSA-rapport 04-2025
Radioaktivitet i dyr på utmarksbeite 2023
- 5 DSA-rapport 05-2025
**IRRS Follow-up Mission, 2025
Advance Reference Material
Summary Report v.3**
- 6 DSA-rapport 06-2025
**Dispersion of Radioactive Contaminants from the Komsomolets Submarine
Dispersion of Radioactive Contaminants from the Komsomolets Submarine under Climate and Environmental Change Scenarios**